Progress In Electromagnetics Research, PIER 33, 261–298, 2001

PLANE WAVE SCATTERING BY AN ACHIRAL MULTILAYERED SPHERE IN AN INFINITELY EXTENDED CHIRAL HOST MEDIUM

L.-W. Li, Y. Dan, M.-S. Leong, and T.-S. Yeo

Department of Electrical and Computer Engineering
The National University of Singapore
10 Kent Ridge Crescent, Singapore 119260

J. A. Kong

Department of Electrical Engineering and Computer Science
Massachusetts Institute of Technology
Cambridge, MA 02139, USA

Abstract—An analytic solution to the problem of plane wave scattering by an achiral multilayered sphere in a host chiral medium is obtained in this paper. By applying the radiation-to-scattering transform, the scattering problem can be considered as the specific radiation problems where the radiated source equivalent to the electromagnetic plane wave is located at infinity. The volumetric currents which generate right circular polarization (RCP) and left circular polarization (LCP) plane waves, respectively, are found. An integral equation consisting the volumetric current distributions and the dyadic Green's functions is formulated to obtain both the equivalent incident wave fields and the scattered fields. Two-layered lossless and lossy dielectric spheres and a conducting sphere with a dielectric coated layer buried in an infinitely extended host chiral medium are considered and the expressions for the scattered fields in far-zone are found in explicit analytic form. The characteristics of scattered fields are illustrated and discussed in terms of the circular polarization degree and linear polarization degree against different chiral admittances and sizes.

1. INTRODUCTION

Chiral media, which were discovered in the last century, have been of much interest to researchers in many different fields (*e.g.*, physics, chemistry, and biology). The lack of the symmetry between the object and its mirror image is referred as chirality (handedness). Because of the coupling between the electric and magnetic fields, more complicated relationships between the electric- and the magnetic-fields have been developed for analyzing the behavior of the macroscopic electromagnetic fields in such an environment. During the past a few decades, much attention has been focused on the interaction of electromagnetic fields with chiral media, motivated by numerous applications in the fields of antennas, waveguide propagation, radio wave scattering, and microwave device designs. There has been a lot of research work contributing significantly to this field, involving chiral media, for instance, in [1–11].

Electromagnetic wave scattering from a chiral object in an achiral environment has been well documented. Exact or analytic solutions for electromagnetic scattering by a chiral sphere [12–14, 11], circular cylinder(s) [15–18], spherical shells [19], and a spheroid [20] are available in literature. However, the problem of an achiral object buried in a chiral environment have not been well studied, to our best knowledge. The only representative references available in this topic are (1) a theoretical and numerical analysis of an achiral object buried in a chiral background using the Born approximation from the volumetric integral equation method by Lindell and Silverman [21], (2) theoretical formulations of an achiral dielectric sphere [22] and a coated dielectric sphere [23, 22] both buried in a chiral background using the matched boundary conditions, and (3) a theoretical formulation of a homogeneous chiral scatterer immersed in another homogeneous chiral medium using the transition matrix (T-matrix) method [24]. It should be pointed out that (1) the results obtained in [21] are only approximately valid because of the Born approximation and they do not hold when size of the object is comparable with, or larger than, the operating wavelength; (2) the work in either [23] or [22] contains only theoretical formulation and there is no numerical results obtained and presented, so that there lacks of the verification of the correctness and validation; and (3) the T-matrix method applied in [24] is a computational technique, and numerical algorithms for implementing the formulae into programme codes are quite essential and numerical results are necessary (i) to check whether the formulation is correct and valid over a wide frequency spectrum and a large dimension range and (ii) to show how accurate, efficient, and fast the programme is. All the above thus motivate the re-visit of this paper to the problem. Different from the previous analysis this paper employs a full-wave technique to analyse this problem both theoretically and numerically. The theoretical formulation in this work is such made by extending a recently developed radiation-to-scattering transform technique that the derivation becomes very straightforward and easy and numerical solution gets convenient. Most importantly, an analytic resolution to this problem is obtained using this technique, and a comprehensive numerical study of this problem is carried out so as to reveal some new physical phenomena.

In this present paper, we utilize the radiation-to-scattering transform to find the scattered field more accurately. According to radiation-to-scattering transform [25], the scattering problem can be considered as the specific radiation problems where the radiating source is located at infinity which generates the plane wave. Since the wave equation in the unbounded chiral media can be decoupled to the

*r*ight- and *l*eft-handed *c*ircularly *p*olarized (RCP and LCP) waves, the incident wave can be expressed as the sum of RCP and LCP waves and linearly polarized wave under certain conditions. The volumetric currents at infinity which generate respectively the RCP and LCP waves are found and the incident RCP and LCP waves in the infinitely extended chiral medium are expanded in terms of spherical harmonics. The dyadic Green's functions for the unbounded chiral medium and multilayered spherically chiral media are available in [26, 27, 10]. The dyadic Green's function for a conducting sphere with a dielectric coated layer buried in a chiral host medium is represented in this paper. The scattered field can be obtained by integrating the dyadic Green's function for a multilayered chiral sphere and the volumetric current distribution located at infinity. To check the algorithm for verification of correctness, electromagnetic scattering by an achiral sphere in a chiral medium is first calculated and its results are compared with those in [21]. After that, two cases are considered, one is a two-layered dielectric sphere (lossy or lossless) in a host chiral medium and the other is a conducting sphere with a dielectric coated layer in an infinitely extended host chiral medium.

The paper is organized in the order given subsequently. In Subsection 2.1, the coupled wavefield equations in a chiral medium are decoupled. The dyadic Green's functions for a multilayered achiral sphere as well as for a conducting sphere with a dielectric coated layer in the infinitely extended chiral medium are *newly* obtained in Subsections 2.2 and 2.3. The sources located at infinity which generate incident waves with different polarizations are formulated in Subsection 2.4. Incident waves and scattered fields are expressed in Subsections 2.5 and 2.6, respectively. Numerical results of the circular polarization degree and linear polarization degree are obtained and their physical significance is discussed in Section 3.

2. FORMULATION OF THE PROBLEM

2.1. Wave Equations in Chiral Media

Consider an N-layered achiral sphere in an infinitely extended host chiral medium. In the following analysis the time dependence, $e^{-i\omega t}$, is assumed but suppressed throughout the paper. The chiral medium is usually characterized by the following set of constitutive relations [1–3, 5, 9]:

$$\boldsymbol{D} = \varepsilon_1 \boldsymbol{E} - i\chi_1 \boldsymbol{H}, \tag{1a}$$

$$\boldsymbol{B} = \mu_1 \boldsymbol{H} + i\chi_1 \boldsymbol{E}. \tag{1b}$$

where ε_1, μ_1, and χ_1 are the medium's permittivity, permeability and chirality parameter, respectively. If ε_1, μ_1 or χ_1 are complex, the media is lossy. If χ_1=0, then (1a) and (1b) reduce to the constitutive relations for an isotropic achiral medium.

In a chiral medium without source distributions, the wave equation with constitutive relation is

$$\nabla^2 \begin{bmatrix} \boldsymbol{E} \\ \boldsymbol{H} \end{bmatrix} + [\boldsymbol{k}]^2 \begin{bmatrix} \boldsymbol{E} \\ \boldsymbol{H} \end{bmatrix} = 0, \tag{2a}$$

where

$$[\boldsymbol{k}] = \begin{bmatrix} -\omega\chi_1 & -j\omega\mu_1 \\ j\omega\epsilon_1 & -\omega\chi_1 \end{bmatrix}. \tag{2b}$$

By following Bohren [12], the coupling caused by $[\boldsymbol{k}]$ in the wave equation can be removed by diagonalizing $[\boldsymbol{k}]$ such that

$$[\boldsymbol{A}]^{-1}[\boldsymbol{k}][\boldsymbol{A}] = \begin{bmatrix} -k_R & 0 \\ 0 & k_L \end{bmatrix}. \tag{3}$$

A simple form of $[\boldsymbol{A}]$ is then found to be

$$[\boldsymbol{A}] = \begin{bmatrix} 1 & 1 \\ -\frac{j}{\eta_1} & \frac{j}{\eta_1} \end{bmatrix} \tag{4}$$

with the chiral wave impedance given by:

$$\eta_1 = \sqrt{\frac{\mu_1}{\epsilon_1}}. \tag{5}$$

The propagation constant k_1 in the chiral medium is designated generally as

$$k_1^2 = \omega^2(\mu_1\varepsilon_1 - \chi_1), \tag{6}$$

and the symbol ξ_1 is defined by

$$\xi_1 = \omega\chi_1. \tag{7}$$

Hence, there are two circularly polarized modes present in the unbounded medium, *i.e.*, the *r*ight- and *l*eft-handed *c*ircularly *p*olarized (RCP and LCP) waves. Their corresponding wave numbers are given by

$$k_1^{(R)} = \xi_1 + \omega\sqrt{\mu_1\varepsilon_1}, \tag{8a}$$

$$k_1^{(L)} = -\xi_1 + \omega\sqrt{\mu_1\varepsilon_1}. \tag{8b}$$

Define $(\boldsymbol{E}^{(R)}, \boldsymbol{E}^{(L)})$ as

$$\begin{bmatrix} \boldsymbol{E} \\ \boldsymbol{H} \end{bmatrix} = [\boldsymbol{A}] \begin{bmatrix} \boldsymbol{E}^{(R)} \\ \boldsymbol{E}^{(L)} \end{bmatrix}. \tag{9}$$

It has been shown that $\boldsymbol{E}^{(R)}$ and $\boldsymbol{E}^{(L)}$ are the electric fields of right- and left-handed circularly polarized waves with propagation constants $k_1^{(R)}$ and $k_1^{(L)}$. Thus the decoupled source-free wave equation in chiral media is:

$$\nabla^2 \begin{bmatrix} \boldsymbol{E}^{(R)} \\ \boldsymbol{E}^{(L)} \end{bmatrix} + \begin{bmatrix} (k_1^{(R)})^2 \boldsymbol{E}^{(R)} \\ (k_1^{(L)})^2 \boldsymbol{E}^{(L)} \end{bmatrix} = 0. \tag{10}$$

2.2. Dyadic Green's Function for a Multilayered Chiral Sphere

The dyadic Green's function expanded in terms of the modified spherical vector wave functions for a unbounded chiral medium is given [10] in the region $r \gtrless r'$ by:

$$\begin{aligned} \overline{\boldsymbol{G}}_{0e}(\boldsymbol{r}, \boldsymbol{r'}) \;=\; & -\frac{\widehat{\boldsymbol{r}}\widehat{\boldsymbol{r}}}{k_f^2}\delta(\boldsymbol{r}-\boldsymbol{r}') + \frac{i}{2\pi(k_s^{(R)}+k_s^{(l)})} \\ & \cdot \sum_{m,n}(2-\delta_0)\frac{(2n+1)(n-m)!}{n(n+1)(n+m)!} \\ & \cdot \left\{ \begin{array}{l} \left[k_s^{(R)}\right]^2 \boldsymbol{V}^{(1)}_{\substack{e\\o}mn}(k_s^{(R)})\boldsymbol{V}'_{\substack{e\\o}mn}(k_s^{(R)}) \\ \qquad\qquad + \left[k_s^{(L)}\right]^2 \boldsymbol{W}^{(1)}_{\substack{e\\o}mn}(k_s^{(L)})\boldsymbol{W}'_{\substack{e\\o}mn}(k_s^{(L)}), \\ \left[k_s^{(R)}\right]^2 \boldsymbol{V}_{\substack{e\\o}mn}(k_s^{(R)})\boldsymbol{V}'^{(1)}_{\substack{e\\o}mn}(k_s^{(R)}) \\ \qquad\qquad + \left[k_s^{(L)}\right]^2 \boldsymbol{W}_{\substack{e\\o}mn}(k_s^{(L)})\boldsymbol{W}'^{(1)}_{\substack{e\\o}mn}(k_s^{(L)}), \end{array} \right. \end{aligned} \tag{11}$$

where the prime denotes the coordinates (r', θ', ϕ') of the current source $\boldsymbol{J}_f$, m and n identify the eigenvalue parameters, and $\delta_0 = 1$ for $m = 0$ or $n = 0$ and $\delta_0 = 0$ otherwise. The superscript (3) denotes that the third type of spherical Bessel function or the first type of spherical Hankel function $h_n^{(1)}(\rho)$ should be chosen in the expression of the spherical wave vector functions, otherwise the first type of spherical Bessel function should be chosen as the spherical function instead.

The dyadic Green's function for a spherically multilayered chiral medium can be found in [10]. Since the source is in the outermost layer with subscript 1 which is a chiral layer, the scattering dyadic Green's function can be reduced to:

$$\begin{aligned}\overline{\boldsymbol{G}}_{es}^{(11)}(\boldsymbol{r},\boldsymbol{r'}) &= \frac{i}{2\pi\left(k_1^{(R)}+k_1^{(L)}\right)}\sum_{m,n}(2-\delta_0)\frac{(2n+1)(n-m)!}{n(n+1)(n+m)!} \\ &\cdot\Big\{\mathcal{C}_{12}^{11}\boldsymbol{V}_{\substack{e\\o}mn}^{(3)}\left(k_1^{(R)}\right)\boldsymbol{V}_{\substack{e\\o}mn}^{\prime(3)}\left(k_1^{(R)}\right) \\ &+\mathcal{C}_{22}^{11}\boldsymbol{W}_{\substack{e\\o}mn}^{(3)}\left(k_1^{(L)}\right)\boldsymbol{V}_{\substack{e\\o}mn}^{\prime(3)}\left(k_1^{(R)}\right) \\ &+\mathcal{C}_{14}^{11}\boldsymbol{V}_{\substack{e\\o}mn}^{(3)}\left(k_1^{(R)}\right)\boldsymbol{W}_{\substack{e\\o}mn}^{\prime(3)}\left(k_1^{(L)}\right) \\ &+\mathcal{C}_{24}^{11}\boldsymbol{W}_{\substack{e\\o}mn}^{(3)}\left(k_1^{(L)}\right)\boldsymbol{W}_{\substack{e\\o}mn}^{\prime(3)}\left(k_1^{(L)}\right)\Big\}. \end{aligned} \tag{12}$$

In Eqs. (11) and (12), the normalized spherical vector wave functions are defined as

$$\boldsymbol{V}_{\substack{e\\o}mn}(k) = \frac{\boldsymbol{M}_{\substack{e\\o}mn}(k)+\boldsymbol{N}_{\substack{e\\o}mn}(k)}{\sqrt{2}}, \tag{13a}$$

$$\boldsymbol{W}_{\substack{e\\o}mn}(k) = \frac{\boldsymbol{M}_{\substack{e\\o}mn}(k)-\boldsymbol{N}_{\substack{e\\o}mn}(k)}{\sqrt{2}}, \tag{13b}$$

where the vector spherical wave functions are written as:

$$\begin{aligned}\boldsymbol{M}_{\substack{e\\o}mn}(k) &= \mp\frac{mz_n(kr)}{\sin\theta}P_n^m(\cos\theta)\begin{matrix}\sin\\\cos\end{matrix}m\phi\widehat{\boldsymbol{\theta}} \\ &\quad -z_n(kr)\frac{\partial P_n^m(\cos\theta)}{\partial\theta}\begin{matrix}\cos\\\sin\end{matrix}m\phi\widehat{\boldsymbol{\phi}}, \end{aligned} \tag{14a}$$

$$\begin{aligned}\boldsymbol{N}_{\substack{e\\o}mn}(k) &= \frac{n(n+1)z_n(kr)}{kr}P_n^m(\cos\theta)\begin{matrix}\cos\\\sin\end{matrix}m\phi\widehat{\boldsymbol{r}} \\ &\quad +\frac{\partial[rz_n(kr)]}{kr\partial r}\frac{\partial P_n^m(\cos\theta)}{\partial\theta}\begin{matrix}\cos\\\sin\end{matrix}m\phi\widehat{\boldsymbol{\theta}} \\ &\quad \mp\frac{m}{\sin\theta}\frac{\partial[rz_n(kr)]}{kr\partial r}P_n^m(\cos\theta)\begin{matrix}\sin\\\cos\end{matrix}m\phi\widehat{\boldsymbol{\phi}}, \end{aligned} \tag{14b}$$

where $z_n(kr)$ represents the spherical Bessel functions of order n, and $P_n^m(\cos\theta)$ identifies the associated Legendre function of the first kind with the order (n,m). The scattering coefficients defined as above can be found in Appendix A.

2.3. Dyadic Green's Function for a Conducting Sphere Coated with a Dielectric Layer

Based on radiation-to-scattering transform [25], when considering the scattering by a conductor sphere covered with a dielectric out layer in chiral host medium, the dyadic Green's function should be obtained at first. Using the method of scattering superposition, we write the dyadic Green's function as follows:

$$\overline{\boldsymbol{G}}_e^{(fs)}(\boldsymbol{r},\boldsymbol{r'}) = \overline{\boldsymbol{G}}_{e0}(\boldsymbol{r},\boldsymbol{r'})\delta_f^s + \overline{\boldsymbol{G}}_{es}^{(fs)}(\boldsymbol{r},\boldsymbol{r'}), \tag{15}$$

where the superscript (fs) denotes the cases where the field point (in the f^{th}-region) and source point (in the s^{th}-region) are located, respectively, while the subscript s identifies the scattering dyadic Green's function. Since the source is located in the outmost region in which the parameters are denoted by the subscript 1, we can write the dyadic Green's function in the dielectric layer as:

$$\begin{aligned}
&\overline{\boldsymbol{G}}_e^{(21)}(\boldsymbol{r},\boldsymbol{r'}) \\
= \;& \frac{i}{4\pi k_0}\sum_{m,n}(2-\delta_0)\frac{(2n+1)(n-m)!}{n(n+1)(n+m)!} \\
&\cdot\Big\{\mathcal{C}_{12}^{11}\boldsymbol{V}_{\substack{e\\o}mn}^{(3)}(k_2)\boldsymbol{V}_{\substack{e\\o}mn}^{\prime(3)}(k_2) + \mathcal{C}_{22}^{11}\boldsymbol{W}_{\substack{e\\o}mn}^{(3)}(k_2)\boldsymbol{V}_{\substack{e\\o}mn}^{\prime(3)}(k_2) \\
&+\mathcal{C}_{14}^{11}\boldsymbol{V}_{\substack{e\\o}mn}^{(3)}(k_2)\boldsymbol{W}_{\substack{e\\o}mn}^{\prime(3)}(k_2) + \mathcal{C}_{24}^{11}\boldsymbol{W}_{\substack{e\\o}mn}^{(3)}(k_2)\boldsymbol{W}_{\substack{e\\o}mn}^{\prime(3)}(k_2) \\
&+\mathcal{C}_{32}^{11}\boldsymbol{V}_{\substack{e\\o}mn}(k_2)\boldsymbol{V}_{\substack{e\\o}mn}^{\prime(3)}(k_2) + \mathcal{C}_{42}^{11}\boldsymbol{W}_{\substack{e\\o}mn}(k_2)\boldsymbol{V}_{\substack{e\\o}mn}^{\prime(3)}(k_2) \\
&+\mathcal{C}_{34}^{11}\boldsymbol{V}_{\substack{e\\o}mn}(k_2)\boldsymbol{W}_{\substack{e\\o}mn}^{\prime(3)}(k_2) + \mathcal{C}_{44}^{11}\boldsymbol{W}_{\substack{e\\o}mn}(k_2)\boldsymbol{W}_{\substack{e\\o}mn}^{\prime(3)}(k_2)\Big\},
\end{aligned} \tag{16}$$

where $k_2 = \omega\mu_2\epsilon_2$ is the wave number in the dielectric coated region which is denoted by subscript 2. In the outmost region, the dyadic Green's function is expressed:

$$\begin{aligned}
\overline{\boldsymbol{G}}_e^{(11)}(\boldsymbol{r},\boldsymbol{r'}) \;=\; & \frac{i}{2\pi\left(k_1^{(R)}+k_1^{(L)}\right)}\sum_{m,n}(2-\delta_0)\frac{(2n+1)(n-m)!}{n(n+1)(n+m)!} \\
&\cdot\Big\{(k_1^R)^2\boldsymbol{V}_{\substack{e\\o}mn}\left(k_1^{(R)}\right)\boldsymbol{V}_{\substack{e\\o}mn}^{\prime(3)}\left(k_1^{(R)}\right) \\
&+(k_1^L)^2\boldsymbol{W}_{\substack{e\\o}mn}\left(k_1^{(L)}\right)\boldsymbol{W}_{\substack{e\\o}mn}^{\prime(3)}\left(k_1^{(R)}\right) \\
&+\mathcal{C}_{12}^{11}\boldsymbol{V}_{\substack{e\\o}mn}^{(3)}\left(k_1^{(R)}\right)\boldsymbol{V}_{\substack{e\\o}mn}^{\prime(3)}\left(k_1^{(R)}\right)
\end{aligned}$$

$$
\begin{aligned}
&+\mathcal{C}_{22}^{11}\boldsymbol{W}_{\substack{e\\o}mn}^{(3)}\left(k_1^{(L)}\right)\boldsymbol{V}_{\substack{e\\o}mn}^{\prime(3)}\left(k_1^{(R)}\right)\\
&+\mathcal{C}_{14}^{11}\boldsymbol{V}_{\substack{e\\o}mn}^{(3)}\left(k_1^{(R)}\right)\boldsymbol{W}_{\substack{e\\o}mn}^{\prime(3)}\left(k_1^{(L)}\right)\\
&+\mathcal{C}_{24}^{11}\boldsymbol{W}_{\substack{e\\o}mn}^{(3)}\left(k_1^{(L)}\right)\boldsymbol{W}_{\substack{e\\o}mn}^{\prime(3)}\left(k_1^{(L)}\right)\Big\}. \qquad (17)
\end{aligned}
$$

Assume the radius of the conducting sphere is a and the thickness of the dielectric coated layer is $b-a$. The electric type of DGF satisfies the following boundary conditions at the spherical interfaces at $r=a$ and $r=b$ in the layered structure:

$$
\begin{aligned}
\widehat{\boldsymbol{r}}\times\overline{\boldsymbol{G}}_e^{(21)}|_{r=a} &= 0, &(18a)\\
\widehat{\boldsymbol{r}}\times\overline{\boldsymbol{G}}_e^{(11)}\Big|_{r=b} &= \widehat{\boldsymbol{r}}\times\overline{\boldsymbol{G}}_e^{(11)}\Big|_{r=b}, &(18b)\\
\frac{1}{\mu_1}\widehat{\boldsymbol{r}}\times\left[\boldsymbol{\nabla}\times\overline{\boldsymbol{G}}_e^{(11)}-\xi_1\overline{\boldsymbol{G}}_e^{(11)}\right]\Big|_{r=b} &= \frac{1}{\mu_2}\widehat{\boldsymbol{r}}\times\left[\boldsymbol{\nabla}\times\overline{\boldsymbol{G}}_e^{(21)}\right]\Big|_{r=b}. &(18c)
\end{aligned}
$$

The scattering coefficients can be determined from the above equations. The complete expressions for scattering coefficients are omitted here due to their lengthy expressions. The numerical calculations can be readily achieved by using the software of Mathematica$^{\mathrm{TM}}$ [28].

2.4. Sources Located at Infinity Which Generate Plane Waves

By following a procedure similar to that in [29], the assumed source located at infinity can be written as:

$$
\begin{aligned}
\boldsymbol{J}^I(\boldsymbol{r}') &= E_I f(r_0)\delta(\boldsymbol{r}'')\widehat{\boldsymbol{\theta}}\\
&= E_I f(r_0)\frac{\delta(r'')\delta(\theta'')\delta(\phi'')}{[r'']^2\sin\theta''}\widehat{\boldsymbol{\theta}}, &(19a)\\
\boldsymbol{J}^{II}(\boldsymbol{r}') &= E_{II} f(r_0)\delta(\boldsymbol{r}'')\widehat{\boldsymbol{\phi}}\\
&= E_{II} f(r_0)\frac{\delta(r'')\delta(\theta'')\delta(\phi'')}{[r'']^2\sin\theta''}\widehat{\boldsymbol{\phi}}, &(19b)
\end{aligned}
$$

where the superscripts I and II correspond to the parallelly and perpendicularly polarized incident waves, respectively. Furthermore, we have the current sources expressed as:

$$
\begin{bmatrix}\boldsymbol{J}^I(r')\\ \boldsymbol{J}^{II}(r')\end{bmatrix}dr' = f(r_0)\begin{bmatrix}E^I\widehat{\boldsymbol{\theta}}\\ E^{II}\widehat{\boldsymbol{\phi}}\end{bmatrix}\delta(r")\delta(\theta")\delta(\phi")dr"d\theta"d\phi". \qquad (20)
$$

Based on the decoupled wave equation, two kinds of electric sources at infinity [25] are assumed to generate RCP and LCP waves respectively. Hence, Eq. (20) can be written as:

$$\begin{bmatrix} \boldsymbol{J}^{I,R}(r') \\ \boldsymbol{J}^{II,R}(r') \end{bmatrix} dr' = f(r_0)^R \begin{bmatrix} E^{I,R}\widehat{\boldsymbol{\theta}} \\ E^{II,R}\widehat{\boldsymbol{\phi}} \end{bmatrix} \cdot\delta(r")\delta(\theta")\delta(\phi")dr"d\theta"d\phi", \tag{21a}$$

$$\begin{bmatrix} \boldsymbol{J}^{I,L}(r') \\ \boldsymbol{J}^{II,L}(r') \end{bmatrix} dr' = f(r_0)^L \begin{bmatrix} E^{I,L}\widehat{\boldsymbol{\theta}} \\ E^{II,L}\widehat{\boldsymbol{\phi}} \end{bmatrix} \cdot\delta(r")\delta(\theta")\delta(\phi")dr"d\theta"d\phi", \tag{21b}$$

where

$$f(r_0)^{(R,L)} = \frac{i4\pi}{\omega\mu_1} r_0 e^{-ik_1^{(R,L)}r_0}. \tag{22}$$

2.5. Incident Waves

To obtain the incident waves of parallel and perpendicular polarizations, the radiation-to-scattering transform [25] is utilized. Since the host chiral medium is infinitely extended, the assumed source located at infinity can still be adopted. We apply the following integral equation:

$$\boldsymbol{E}^i(r) = i\omega\mu_1 \iiint_A \overline{\boldsymbol{G}}_{e0}(\boldsymbol{r}, \boldsymbol{r'}) \cdot \boldsymbol{J}(\boldsymbol{r'})dV'. \tag{23}$$

According the characteristic of chiral media, the incident waves in host chiral media include RCP and LCP. From the above equation, we can easily obtain the RCP and LCP incident waves. Substitution of Eq. (21) into Eq. (23) leads to $r' \to r_0$, $\theta' \to \alpha$, and $\phi' \to 0$ in the integral containing the vector eigenfunctions $\boldsymbol{M}'_{\substack{e\\o}mn}(k_1^{(R,L)})$ and $\boldsymbol{N}'_{\substack{e\\o}mn}(k_1^{(R,L)})$. Applying the asymptotic form of Hankel function of a large argument gives the following expressions:

$$h_n^{(1)}\left(k_0^{(R,L)}r_0\right) = (-i)^{n+1}\frac{e^{-ik_0^{(R,L)}r_0}}{k_0^{(R,L)}r_0}, \tag{24a}$$

$$\frac{d\left[\left(k_0^{(R,L)}r_0\right)h_n^{(1)}\left(k_0^{(R,L)}r_0\right)\right]}{\left(k_0^{(R,L)}r_0\right)\left(d(k_0^{(R,L)}r_0\right)} = (-i)^n\frac{e^{-ik_0^{(R,L)}r_0}}{k_0^{(R,L)}r_0}. \tag{24b}$$

Finally, the electric fields of the RCP and LCP incident waves are

written as:

$$\begin{aligned}
\boldsymbol{E}_{\ I\ I}^{iR} &= \sum_{n=1}^{\infty}\sum_{m=0}^{n}\Bigg\{A_{I\ II}^{R}{}_{mn}\left[\boldsymbol{M}_{emn}^{(1)}\left(k_1^{(R)}\right)+\boldsymbol{N}_{emn}^{(1)}\left(k_1^{(R)}\right)\right] \\
&\quad +B_{I\ II}^{R}{}_{mn}\left[\boldsymbol{M}_{omn}^{(1)}\left(k_1^{(R)}\right)+\boldsymbol{N}_{omn}^{(1)}\left(k_1^{(R)}\right)\right]\Bigg\}, \qquad (25a)\\
\boldsymbol{E}_{\ I\ I}^{iL} &= \sum_{n=1}^{\infty}\sum_{m=0}^{n}\Bigg\{A_{I\ II}^{L}{}_{mn}\left[\boldsymbol{M}_{emn}^{(1)}\left(k_1^{(L)}\right)-\boldsymbol{N}_{emn}^{(1)}\left(k_1^{(L)}\right)\right] \\
&\quad +B_{I\ II}^{L}{}_{mn}\left[\boldsymbol{M}_{omn}^{(1)}\left(k_1^{(L)}\right)-\boldsymbol{N}_{omn}^{(1)}\left(k_1^{(L)}\right)\right]\Bigg\}, \qquad (25b)
\end{aligned}$$

where

$$\begin{aligned}
A_{I\ II}^{R,L}{}_{mn} &= \frac{k_1^{(R,L)}}{2\omega\sqrt{\mu\epsilon}}(-i)^n(2-\delta_{m0})\mathcal{N}_{mn} \\
&\quad \cdot\begin{Bmatrix} -i\dfrac{\partial P_n^m(\cos\alpha)}{\partial\alpha}E^{I(R,L)} \\ \dfrac{\partial P_n^m(\cos\alpha)}{\partial\alpha}E^{II(R,L)} \end{Bmatrix}, \qquad (26a)\\
B_{I\ II}^{R,L}{}_{mn} &= \frac{k_1^{(R,L)}}{2\omega\sqrt{\mu\epsilon}}(-i)^n(2-\delta_{m0})\mathcal{N}_{mn} \\
&\quad \cdot\begin{Bmatrix} -\dfrac{mP_n^m(\cos\alpha)}{\sin\alpha}E^{I(R,L)} \\ -i\dfrac{mP_n^m(\cos\alpha)}{\sin\alpha}E^{II(R,L)} \end{Bmatrix}. \qquad (26b)
\end{aligned}$$

If we consider the incident waves along the positive $\hat{\boldsymbol{z}}$-direction, the expressions of the incident waves can be reduced to:

$$\begin{aligned}
\boldsymbol{E}_{\ I\ I}^{iR} &= \sum_{n=1}^{\infty}\Bigg\{A_{I\ II}^{R}{}_{n}\left[\boldsymbol{M}_{e1n}^{(1)}\left(k_1^{(R)}\right)+\boldsymbol{N}_{e1n}^{(1)}\left(k_1^{(R)}\right)\right] \\
&\quad +B_{I\ II}^{R}{}_{n}\left[\boldsymbol{M}_{o1n}^{(1)}\left(k_1^{(R)}\right)+\boldsymbol{N}_{o1n}^{(1)}\left(k_1^{(R)}\right)\right]\Bigg\}, \qquad (27a)\\
\boldsymbol{E}_{\ I\ I}^{iL} &= \sum_{n=1}^{\infty}\Bigg\{A_{I\ II}^{L}{}_{n}\left[\boldsymbol{M}_{e1n}^{(1)}\left(k_1^{(L)}\right)-\boldsymbol{N}_{e1n}^{(1)}\left(k_1^{(L)}\right)\right] \\
&\quad +B_{I\ II}^{L}{}_{n}\left[\boldsymbol{M}_{o1n}^{(1)}\left(k_1^{(L)}\right)-\boldsymbol{N}_{o1n}^{(1)}\left(k_1^{(L)}\right)\right]\Bigg\}, \qquad (27b)
\end{aligned}$$

where

$$A_{\substack{I\\II}n}^{R,L} = \frac{k_1^{(R,L)}}{\omega\sqrt{\mu\epsilon}} i^n \frac{2n+1}{n(n+1)} \left\{ \begin{array}{c} -iE^{I(R,L)} \\ E^{II(R,L)} \end{array} \right\}, \tag{28a}$$

$$B_{\substack{I\\II}n}^{R,L} = \frac{k_1^{(R,L)}}{\omega\sqrt{\mu\epsilon}} i^n \frac{2n+1}{n(n+1)} \left\{ \begin{array}{c} E^{I(R,L)} \\ iE^{II(R,L)} \end{array} \right\}. \tag{28b}$$

It is observed that in [21] the incident waves are the same as those of parallel polarization considered here. As for the perpendicular polarization, the results given here are newly obtained. When $k_1^R E^R = k_1^L E^L$, the left- and right-handed circular polarizations of the incident wave reduce to a linear polarization.

2.6. Scattered Fields

To obtain the scattered field, the following integral equation is usually employed:

$$\boldsymbol{E}^s(r) = i\omega\mu_1 \iiint_A \overline{\boldsymbol{G}}_{es}(\boldsymbol{r}, \boldsymbol{r'}) \cdot \boldsymbol{J}(\boldsymbol{r'}) dV'. \tag{29}$$

By following the same procedure for obtaining the incident waves as in [29], the scattered fields can be easily found. Corresponding to the RCP and LCP incident waves, the scattered fields are obtained respectively as follows:

$$\begin{aligned} \boldsymbol{E}_{\substack{I\\II}}^{s,iR} = {} & \frac{k_1^{(R)}}{2\omega\sqrt{\mu\epsilon}} \left[\begin{array}{c} E^{I,R} \\ E^{II,R} \end{array} \right] \sum_{n=1}^{\infty} (-i)^n (2-\delta_{m0}) \mathcal{N}_{mn} \\ & \cdot \left\{ \mathcal{X}_{12} \left[\begin{array}{c} -i\dfrac{\partial P_n^m(\cos\alpha)}{\partial\alpha} \\ -i\dfrac{mP_n^m(\cos\alpha)}{\sin\alpha} \end{array} \right] \left[\boldsymbol{M}_{\substack{e\\o}mn}\left(k_1^R\right) + \boldsymbol{N}_{\substack{e\\o}mn}\left(k_1^R\right) \right] \right. \\ & + \mathcal{X}_{22} \left[\begin{array}{c} -i\dfrac{\partial P_n^m(\cos\alpha)}{\partial\alpha} \\ -i\dfrac{mP_n^m(\cos\alpha)}{\sin\alpha} \end{array} \right] \left[\boldsymbol{M}_{\substack{e\\o}mn}\left(k_1^L\right) - \boldsymbol{N}_{\substack{e\\o}mn}\left(k_1^L\right) \right] \\ & + \mathcal{X}_{12} \left[\begin{array}{c} -\dfrac{mP_n^m(\cos\alpha)}{\sin\alpha} \\ \dfrac{\partial P_n^m(\cos\alpha)}{\partial\alpha} \end{array} \right] \left[\boldsymbol{M}_{\substack{o\\e}mn}\left(k_1^R\right) + \boldsymbol{N}_{\substack{o\\e}mn}\left(k_1^R\right) \right] \\ & \left. + \mathcal{X}_{22} \left[\begin{array}{c} -\dfrac{mP_n^m(\cos\alpha)}{\sin\alpha} \\ \dfrac{\partial P_n^m(\cos\alpha)}{\partial\alpha} \end{array} \right] \left[\boldsymbol{M}_{\substack{o\\e}mn}\left(k_1^L\right) - \boldsymbol{N}_{\substack{o\\e}mn}\left(k_1^L\right) \right] \right\}, \end{aligned} \tag{30a}$$

$$\boldsymbol{E}_{\substack{I\\II}}^{s,iL} = \frac{k_1^{(L)}}{2\omega\sqrt{\mu\epsilon}} \begin{bmatrix} E^{I,L} \\ E^{II,L} \end{bmatrix} \sum_{n=1}^{\infty} (-i)^n (2-\delta_{m0}) \mathcal{N}_{mn}$$
$$\cdot \left\{ \mathcal{X}_{14} \begin{bmatrix} i\dfrac{\partial P_n^m(\cos\alpha)}{\partial\alpha} \\ i\dfrac{mP_n^m(\cos\alpha)}{\sin\alpha} \end{bmatrix} \left[\boldsymbol{M}_{\substack{e\\o}mn}\left(k_1^R\right) + \boldsymbol{N}_{\substack{e\\o}mn}\left(k_1^L\right) \right] \right.$$
$$+\mathcal{X}_{24} \begin{bmatrix} i\dfrac{\partial P_n^m(\cos\alpha)}{\partial\alpha} \\ i\dfrac{mP_n^m(\cos\alpha)}{\sin\alpha} \end{bmatrix} \left[\boldsymbol{M}_{\substack{e\\o}mn}\left(k_1^L\right) - \boldsymbol{N}_{\substack{e\\o}mn}\left(k_1^L\right) \right]$$
$$+\mathcal{X}_{14} \begin{bmatrix} -\dfrac{mP_n^m(\cos\alpha)}{\sin\alpha} \\ \dfrac{\partial P_n^m(\cos\alpha)}{\partial\alpha} \end{bmatrix} \left[\boldsymbol{M}_{\substack{o\\e}mn}\left(k_1^R\right) + \boldsymbol{N}_{\substack{o\\e}mn}\left(k_1^R\right) \right]$$
$$\left. + \mathcal{X}_{24} \begin{bmatrix} -\dfrac{mP_n^m(\cos\alpha)}{\sin\alpha} \\ \dfrac{\partial P_n^m(\cos\alpha)}{\partial\alpha} \end{bmatrix} \left[\boldsymbol{M}_{\substack{o\\e}mn}\left(k_1^L\right) - \boldsymbol{N}_{\substack{o\\e}mn}\left(k_1^L\right) \right] \right\}, \quad (30b)$$

where the scattering coefficients are written as follows:

$$\mathcal{X}_{12} = \frac{\mathcal{C}_{12}}{\left(k_1^R\right)^2}, \quad (31a)$$

$$\mathcal{X}_{22} = \frac{\mathcal{C}_{22}}{\left(k_1^R\right)^2}, \quad (31b)$$

$$\mathcal{X}_{14} = \frac{\mathcal{C}_{14}}{\left(k_1^L\right)^2}, \quad (31c)$$

$$\mathcal{X}_{24} = \frac{\mathcal{C}_{24}}{\left(k_1^L\right)^2}. \quad (31d)$$

It is noted that the superscripts iR and iL correspond to the RCP and LCP incident waves, respectively. Also, the RCP and LCP scattered waves are represented, respectively, by different wave numbers, k^R and k^L, in vector wave functions.

3. NUMERICAL RESULTS

3.1. Fundamental Formulae

In general, the interaction between a linearly or circularly polarized incident wave and an achiral sphere in a chiral environment results in

an elliptically polarized scattered wave. In this paper, our numerical computation will be made on the degree of circular polarization τ_C and the degree of linearly polarization τ_L. The physical significances of these physical quantities are readily seen from the following definitions of the degree of circular polarization (which spans the range $-1 \leq \tau_C \leq 1$):

$$\tau_C = \frac{|E_R^s|^2 - |E_L^s|^2}{|E_R^s|^2 + |E_L^s|^2}, \tag{32}$$

and of the degree of linear polarization:

$$\tau_L = \frac{|E^s \cdot E^s|}{E^s \cdot E^{s*}}. \tag{33}$$

Considering the incident wave which is in the positive $\widehat{\boldsymbol{z}}$-direction, the scattered field can be reduced to:

$$\begin{aligned}
\boldsymbol{E}_{\substack{I\\II}}^{s,iR} &= \frac{k_1^{(R)}}{2\omega\sqrt{\mu\epsilon}} \begin{bmatrix} E^{I,R} \\ E^{II,R} \end{bmatrix} \sum_{n=1}^{\infty} i^n (2-\delta_{m0}) \frac{2n+1}{n(n+1)} \\
&\quad \cdot \Bigg\{ \mathcal{X}_{12} \begin{bmatrix} -i \\ i \end{bmatrix} \left[\boldsymbol{M}_{\substack{e\\o}mn}\left(k_1^R\right) + \boldsymbol{N}_{\substack{e\\o}mn}\left(k_1^R\right) \right] \\
&\quad + \mathcal{X}_{22} \begin{bmatrix} -i \\ i \end{bmatrix} \left[\boldsymbol{M}_{\substack{e\\o}mn}\left(k_1^L\right) - \boldsymbol{N}_{\substack{e\\o}mn}\left(k_1^L\right) \right] \\
&\quad + \mathcal{X}_{12} \begin{bmatrix} 1 \\ 1 \end{bmatrix} \left[\boldsymbol{M}_{\substack{o\\e}mn}\left(k_1^R\right) + \boldsymbol{N}_{\substack{o\\e}mn}\left(k_1^R\right) \right] \\
&\quad + \mathcal{X}_{22} \begin{bmatrix} 1 \\ 1 \end{bmatrix} \left[\boldsymbol{M}_{\substack{o\\e}mn}\left(k_1^L\right) - \boldsymbol{N}_{\substack{o\\e}mn}\left(k_1^L\right) \right] \Bigg\}, \qquad (34a) \\
\boldsymbol{E}_{\substack{I\\II}}^{s,iL} &= \frac{k_1^{(L)}}{2\omega\sqrt{\mu\epsilon}} \begin{bmatrix} E^{I,L} \\ E^{II,L} \end{bmatrix} \sum_{n=1}^{\infty} i^n (2-\delta_{m0}) \frac{2n+1}{n(n+1)} \\
&\quad \cdot \Bigg\{ \mathcal{X}_{14} \begin{bmatrix} i \\ -i \end{bmatrix} \left[\boldsymbol{M}_{\substack{e\\o}mn}\left(k_1^R\right) + \boldsymbol{N}_{\substack{e\\o}mn}\left(k_1^L\right) \right] \\
&\quad + \mathcal{X}_{24} \begin{bmatrix} i \\ -i \end{bmatrix} \left[\boldsymbol{M}_{\substack{e\\o}mn}\left(k_1^L\right) - \boldsymbol{N}_{\substack{e\\o}mn}\left(k_1^L\right) \right] \\
&\quad + \mathcal{X}_{14} \begin{bmatrix} 1 \\ 1 \end{bmatrix} \left[\boldsymbol{M}_{\substack{o\\e}mn}\left(k_1^R\right) + \boldsymbol{N}_{\substack{o\\e}mn}\left(k_1^R\right) \right] \\
&\quad + \mathcal{X}_{24} \begin{bmatrix} 1 \\ 1 \end{bmatrix} \left[\boldsymbol{M}_{\substack{o\\e}mn}\left(k_1^L\right) - \boldsymbol{N}_{\substack{o\\e}mn}\left(k_1^L\right) \right] \Bigg\}. \qquad (34b)
\end{aligned}$$

In the first case, for simplicity, we consider the right-handed circularly polarized incident wave due to a current source at infinity of the first

polarization. The amplitude of scattered field can be written as:

$$\left|E^{s(R,L)}\right|^2 = \left|E_\theta^{s(R,L)}\right|^2 + \left|E_\phi^{s(R,L)}\right|^2. \tag{35}$$

By applying the asymptotic expression of spherical Hankel function in Eq. (24), the scattered fields in far-zone are obtained.

Here we consider the scattered fields in far-zone on two principal planes, *i.e.*, the $\phi = 0$ plane and $\phi = \frac{\pi}{2}$ plane. To calculate the degree of circular polarization, we find that the τ_C and τ_L functions are the same in magnitude in $\phi = 0$ plane and $\phi = \frac{\pi}{2}$ plane [21]. For the nomalization purpose, we take $\phi = 0$ and assume $E^{I,R} = E^{II,R}$ to be unity. Thus, we obtain the scattered far-zone fields as follows:

$$E_\theta^{sR} = \frac{1}{\omega\sqrt{\mu\epsilon}r_0}\sum_{n=1}^{\infty}\frac{2n+1}{2n(n+1)}\left\{-i\mathcal{X}_{12}\left[\frac{\partial P_n^1(\cos\theta)}{\partial\theta}+\frac{P_n^1(\cos\theta)}{\sin\theta}\right]\right\}, \tag{36a}$$

$$E_\theta^{sL} = \frac{k^R}{k^L\omega\sqrt{\mu\epsilon}r_0}\sum_{n=1}^{\infty}\frac{2n+1}{2n(n+1)}\left\{i\mathcal{X}_{22}\left[\frac{\partial P_n^1(\cos\theta)}{\partial\theta}-\frac{P_n^1(\cos\theta)}{\sin\theta}\right]\right\}, \tag{36b}$$

$$E_\phi^{sR} = \frac{1}{\omega\sqrt{\mu\epsilon}r_0}\sum_{n=1}^{\infty}\frac{2n+1}{2n(n+1)}\left\{\mathcal{X}_{12}\left[\frac{\partial P_n^1(\cos\theta)}{\partial\theta}+\frac{P_n^1(\cos\theta)}{\sin\theta}\right]\right\}, \tag{36c}$$

$$E_\phi^{sL} = \frac{k^R}{k^L\omega\sqrt{\mu\epsilon}r_0}\sum_{n=1}^{\infty}\frac{2n+1}{2n(n+1)}\left\{\mathcal{X}_{22}\left[\frac{\partial P_n^1(\cos\theta)}{\partial\theta}-\frac{P_n^1(\cos\theta)}{\sin\theta}\right]\right\}. \tag{36d}$$

Based on the above expressions, it is easy to calculate τ_C and τ_L defined in Eq. (32) and Eq. (33), respectively. τ_C and τ_L for the case of only RCP wave incidence are denoted by $\tau_C^{(+)}$ and $\tau_L^{(+)}$.

Secondly, we consider the linearly polarized incident wave. When $E^R k^L = E^L k^R$ [21], the incident wave becomes actually a linearly polarized wave. The τ_C and τ_L are different on two principal planes if the incident wave is linearly polarized. For simplicity, only the expressions of the scattered electric fields due to the first polarized incident wave are included here. The electric fields, when $\phi = 0$, are obtained as follows:

$$\begin{aligned} E_\theta^{sR} &= \frac{1}{k^R\omega\sqrt{\mu\epsilon}r_0}\sum_{n=1}^{\infty}\frac{2n+1}{2n(n+1)}\Bigg[-i(\mathcal{X}_{12}+\mathcal{X}_{14})\frac{P_n^1(\cos\theta)}{\sin\theta} \\ &\quad +(\mathcal{X}_{12}+\mathcal{X}_{14})\frac{\partial P_n^1(\cos\theta)}{\partial\theta}\Bigg], \end{aligned} \tag{37a}$$

$$\begin{aligned} E_\theta^{sL} &= \frac{1}{k^L\omega\sqrt{\mu\epsilon}r_0}\sum_{n=1}^{\infty}\frac{2n+1}{2n(n+1)}\Bigg[-i(\mathcal{X}_{22}+\mathcal{X}_{24})\frac{P_n^1(\cos\theta)}{\sin\theta} \end{aligned}$$

$$-(\mathcal{X}_{22}+\mathcal{X}_{24})\frac{\partial P_n^1(\cos\theta)}{\partial\theta}\Bigg], \tag{37b}$$

$$E_\phi^{sR} = \frac{1}{k^R\omega\sqrt{\mu\epsilon}r_0}\sum_{n=1}^{\infty}\frac{2n+1}{2n(n+1)}\Bigg[(\mathcal{X}_{12}+\mathcal{X}_{14})\frac{P_n^1(\cos\theta)}{\sin\theta} +i(\mathcal{X}_{22}+\mathcal{X}_{24})\frac{\partial P_n^1(\cos\theta)}{\partial\theta}\Bigg], \tag{37c}$$

$$E_\phi^{sL} = \frac{1}{k^L\omega\sqrt{\mu\epsilon}r_0}\sum_{n=1}^{\infty}\frac{2n+1}{2n(n+1)}\Bigg[-(\mathcal{X}_{22}+\mathcal{X}_{24})\frac{P_n^1(\cos\theta)}{\sin\theta} +i(\mathcal{X}_{22}+\mathcal{X}_{24})\frac{\partial P_n^1(\cos\theta)}{\partial\theta}\Bigg]; \tag{37d}$$

and the components of electric fields, when $\phi=\frac{\pi}{2}$, are given by:

$$E_\theta^{sR} = \frac{1}{k^R\omega\sqrt{\mu\epsilon}r_0}\sum_{n=1}^{\infty}\frac{2n+1}{2n(n+1)}\Bigg[(\mathcal{X}_{12}+\mathcal{X}_{14})\frac{\partial P_n^1(\cos\theta)}{\partial\theta} +i(\mathcal{X}_{22}+\mathcal{X}_{24})\frac{P_n^1(\cos\theta)}{\sin\theta}\Bigg], \tag{38a}$$

$$E_\theta^{sL} = \frac{1}{k^L\omega\sqrt{\mu\epsilon}r_0}\sum_{n=1}^{\infty}\frac{2n+1}{2n(n+1)}\Bigg[-(\mathcal{X}_{22}+\mathcal{X}_{24})\frac{\partial P_n^1(\cos\theta)}{\partial\theta} +i(\mathcal{X}_{22}+\mathcal{X}_{24})\frac{P_n^1(\cos\theta)}{\sin\theta}\Bigg], \tag{38b}$$

$$E_\phi^{sR} = \frac{1}{k^R\omega\sqrt{\mu\epsilon}r_0}\sum_{n=1}^{\infty}\frac{2n+1}{2n(n+1)}\Bigg[i(\mathcal{X}_{12}+\mathcal{X}_{14})\frac{\partial P_n^1(\cos\theta)}{\partial\theta} -(\mathcal{X}_{22}+\mathcal{X}_{24})\frac{P_n^1(\cos\theta)}{\sin\theta}\Bigg], \tag{38c}$$

$$E_\phi^{sL} = \frac{1}{k^L\omega\sqrt{\mu\epsilon}r_0}\sum_{n=1}^{\infty}\frac{2n+1}{2n(n+1)}\Bigg[i(\mathcal{X}_{22}+\mathcal{X}_{24})\frac{\partial P_n^1(\cos\theta)}{\partial\theta} +(\mathcal{X}_{22}+\mathcal{X}_{24})\frac{P_n^1(\cos\theta)}{\sin\theta}\Bigg]. \tag{38d}$$

Substituting above expressions to the definitions of τ_C and τ_L, the resultant polarization degrees can be obtained. The corresponding quantities of τ_C and τ_L in the present case are denoted by $\tau_C^{(l)}$ and $\tau_L^{(l)}$.

3.2. A Comparison with Existing Results

To see how the theoretical results are implemented into the programme, to check the corrections of the present formulation, and to examine the validity of the previously published results elsewhere, we have made a comprehensive numerical computation using the Mathematica$^{\text{TM}}$ [28] on, and extensively discussed, the polarization degrees. For ease of comparison with the existing results, we choose the same parameters as in [21] to analyze electromagnetic scattering by a dielectric sphere in a chiral host medium.

As a first check, we have assumed that $\chi_1 = 0$ while $\epsilon_1 = \epsilon_0$ and $\mu_1 = \mu_0$ in free space (for a unbounded free space case) or $\epsilon_1 \neq \epsilon_0$ and $\mu_1 \neq \mu_0$ (for an isotropic dielectric sphere case). It is found from the computational results that the results are simply those reproduced ones for the isotropic media. This means that our results are valid for the specific cases. Also, it partially shows the corrections of the formulation. In addition, we have considered the electromagnetic scattering by electrically very small spheres, for instance, when $ka = 1$ or $a = \lambda/(2\pi)$. The computed results are then compared in Case (a) of Figs. 1 to 4 with those obtained by Lindell and Silverman in [21]. It is apparent that the results obtained using different techniques are in very good agreement, which also partially shows the correctness of the present analysis. After the program codes are checked in detail and the results produced by the codes are examined carefully, we proceed to consider two distinct cases subsequently.

Firstly, we consider the incident wave of only RCP due to the electric source of the first polarization located at infinity. The quantities $\tau_C^{(+)}$ and $\tau_L^{(+)}$ are computed in this paper by the full-wave method and compared with those approximate results obtained by Lindell and Silverman in [21] using the method of integral equation based on the Born approximation, as shown in Fig. 1 and Fig. 2. Following the notation in [21], the $\epsilon_s\epsilon$ and $\mu_s\mu$ represent the material parameters of the achiral sphere while k_r stands for the chiral parameter equal to $\frac{\xi}{k}$. According to the definition of τ_L in Eq. (33), Various τ_L in absolute values are computed and shown in the numerical results.

From Fig. 1 to Fig. 2, it is observed that our results are in good agreement with those by Lindell and Silverman [21] when $ka = 1$. The Born approximation is an approximate method for the scattering problem and it is valid when $2(\epsilon_s - 1)ka \ll 1$ [30], whereas our method is a rigorous method using the full-wave analysis and it is valid for electromagnetic scattering by a sphere of arbitrary dimension. Therefore, our results differ significantly from those by Lindell and

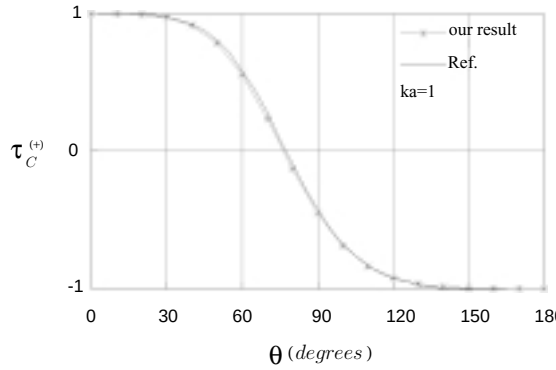

(a) $ka = 1$

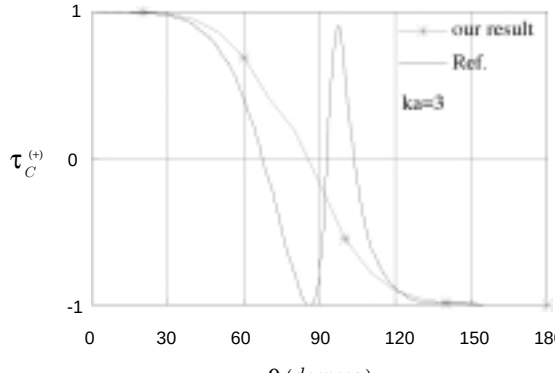

(b) $ka = 3$

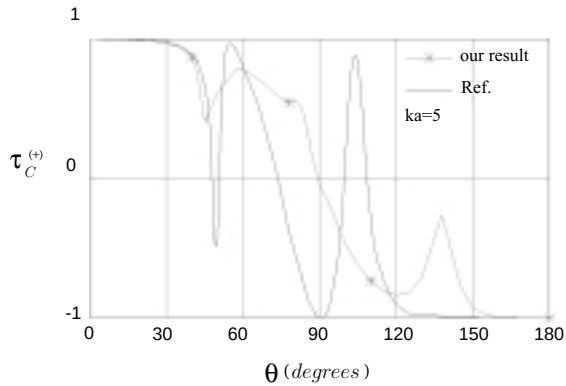

(c) $ka = 5$

Figure 1. Comparison of $\tau_C^{(+)}$ between Lindell and Silverman's and our results. The parameters used are $\varepsilon_s = 1.43,\ \mu_s = 1$, and $k_r = 0.1$.

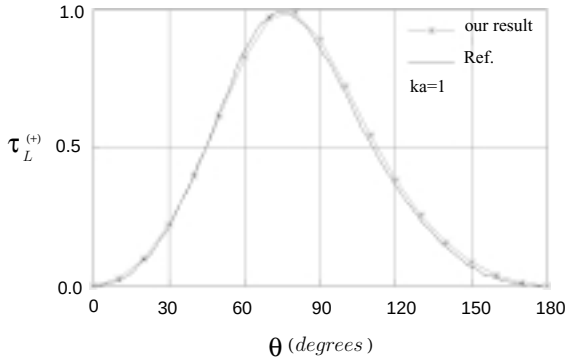

(a) $ka = 1$

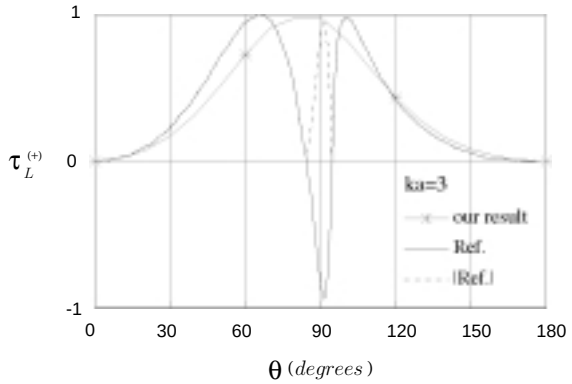

(b) $ka = 3$

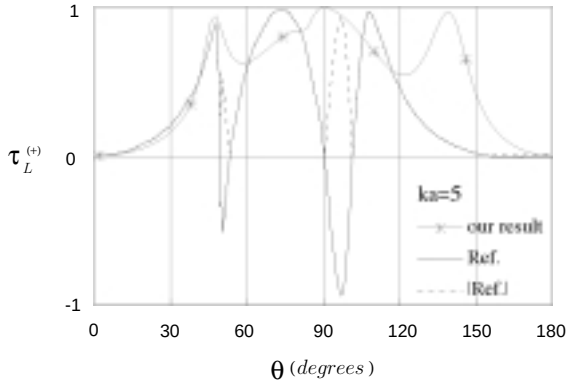

(c) $ka = 5$

Figure 2. Comparison of $\tau_L^{(+)}$ between Lindell and Silverman's and our results. The parameters used are $\varepsilon_s = 1.43$, $\mu_s = 1$, and $k_r = 0.1$.

Silverman [21] (as expected) when the value of ka increases. When the value of ka is very large, our results obtained using the present method are very accurate while those of Lindell and Silverman [21] are no longer valid. This demonstrates the advantage of the present analysis over the previous one in [21].

It is observed from Fig. 1 that the degree of circular polarization varies with the angle of scattering. The degree becomes very large and the directions of polarization are opposite to each other, at $\theta = 0^\circ$ and 180°. When the linear polarization angle θ is about 75°, a linear polarization is expected for $ka = 1$. When ka becomes larger (such as 3 and 5), the the linear polarization angle is getting larger as well (about 80° and 90°, respectively). The linearity and circularity of polarization can also be confirmed from Fig. 2.

Secondly, the incident wave is chosen as a linearly polarized one. The results for $\tau_C^{(l)}$ and $\tau_L^{(l)}$ in $\phi = 0$ and $\phi = \frac{\pi}{2}$ planes are given in Fig. 3 and Fig. 4. Since we calculated the absolute value of τ_L, the curves appearing in $|Ref.|$ are also taken into account in our comparison.

It is again observed in Figs. 3 and 4 that our results are in good agreement with those by Lindell and Silverman [21] when ka is small; but our results are actually very much more accurate than those of Lindell and Silverman [21] especially when the value of ka is very large. Also, it is observed that unlike those given by Lindell and Silverman [21], the degree of linear polarization does not vary so dramatically with the scattering angle. There are a few gradually changed valleys or peaks in the variation; but the levels of the peaks (or valleys) are not so high (or low) as those predicted by Lindell and Silverman [21].

3.3. Scattering by a Two-Layered Dielectric Sphere

Next, we consider a two-layered dielectric sphere in chiral host media. This corresponds a new case for which the numerical results and the physical insight were never obtained and presented elsewhere in literature, to the authors' best knowledge. The incident waves of both RCP and linear polarization due to the source at infinity of the first polarization are chosen. To gain an insight into effects of the sphere's size, different dimensions of the sphere are considered.

3.3.1. Lossless Spheres

The permittivity and permeability of chiral media are set as ϵ and μ and represented by $\epsilon_2 = \epsilon_{s2}\epsilon$, $\mu_2 = \mu_{s2}\mu$, $\epsilon_3 = \epsilon_{s3}\epsilon$ and $\mu_3 = \mu_{s3}\mu$, respectively. The parameters with subscript 3 refer to those in the innermost sphere. Following the denotation in [21], k_r here identifies

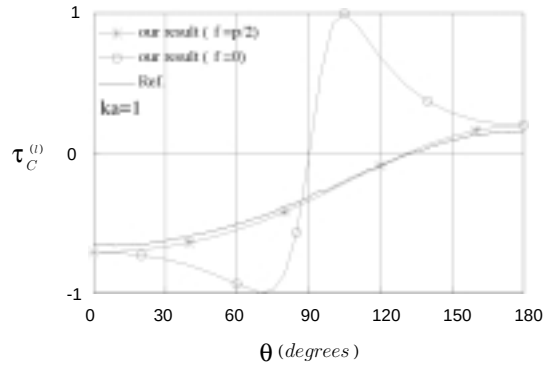

(a) $ka = 1$

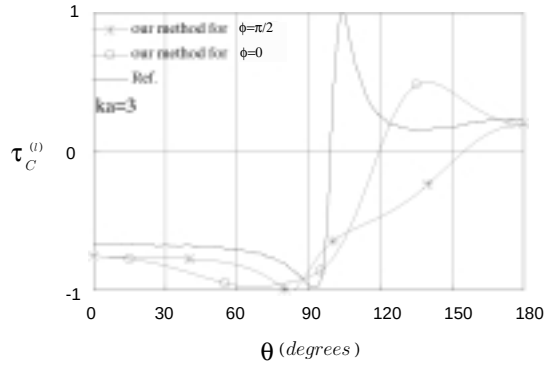

(b) $ka = 3$

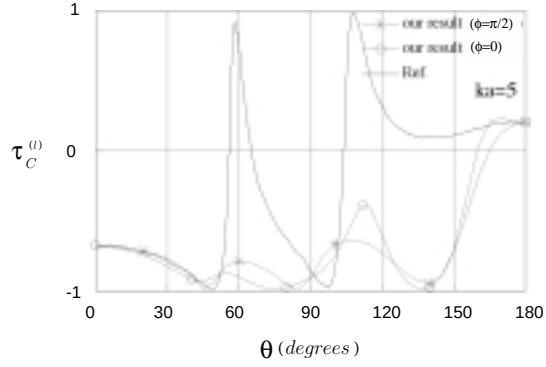

(c) $ka = 5$

Figure 3. Comparison of $\tau_C^{(l)}$ between the results by Lindell and Silverman and by our method. The parameters used are $\varepsilon_s = 1.43$, $\mu_s = 1$, and $k_r = 0.1$.

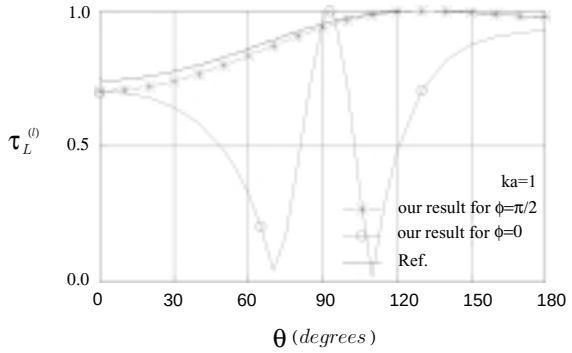

(a) $ka = 1$

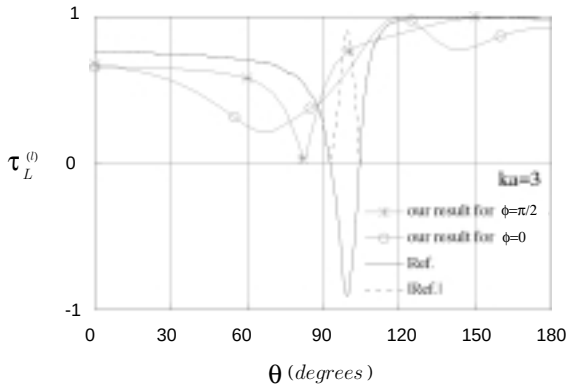

(b) $ka = 3$

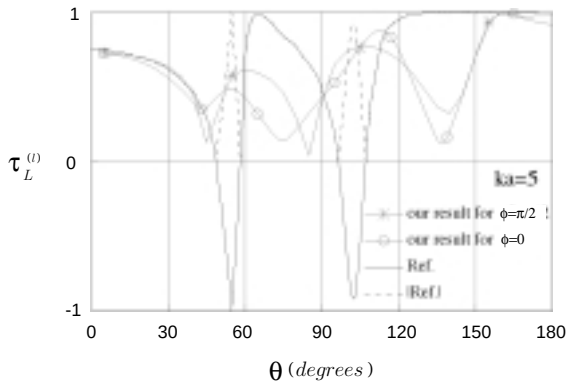

(c) $ka = 5$

Figure 4. Comparison of $\tau_L^{(l)}$ between Lindell and Silverman's and our results. The parameters used are $\varepsilon_s = 1.43$, $\mu_s = 1$, and $k_r = 0.1$.

the chiral parameter. The results for $\tau_C^{(+)}$, $\tau_L^{(+)}$, $\tau_C^{(l)}$ and $\tau_L^{(l)}$ are shown in Figs. 5 and 6. It is observed that if the size of the outer layer is fixed, when the dimension of the inner layer increases, the value of $\tau_C^{(+)}$ increases within the angular range of 0° –130° while the value of $\tau_L^{(+)}$ decreases in the same angular range. On the other hand, if the dimension of the inner layer is constant, when the size of out layer increases, the value of $\tau_C^{(+)}$ decreases and the value of $\tau_L^{(+)}$ increases. When the size of out layer increases, the number of undulatory structures in the plot for $\tau_C^{(+)}$ and $\tau_L^{(+)}$ increases, too.

Physically, it is seen that the outer coating layer plays an important role in determination of the linear and the circular polarizations because both the permittivity and permeability of the outer layer are much larger than those in the inner dielectric sphere. As a result, when the outer layer becomes thinner (saying $b-a \approx \lambda/6$), the outer layer will function like a polarization transformer. But when outer layer is thicker or several times of a half wavelength (i.e., $b - a \approx \lambda/2$), the impedance can be matched so that the outer layer will function as a transparent lens; and in this case, the circular or linear polarization is then determined by the inner spherical resonator. Certainly, the polarization depends then upon the scanning angles, and this variation is shown to be sinusoidally formed.

In Fig. 7, the incident waves of both polarizations are taken into account for the two layer dielectric sphere with $ka = 2$ and $kb = 3$. $\tau_C^{(sl)}$ and $\tau_L^{(sl)}$ represent the results for the case. It is shown that the values of $\tau_C^{(sl)}$ and $\tau_C^{(sl)}$ are greater than $\tau_C^{(l)}$ and$\tau_C^{(l)}$ respectively within the range of 0°–70°, and less in 70°–130°. Furthermore, the undulatory structures of the results of $\tau_C^{(sl)}$ and $\tau_L^{(sl)}$ are shortened when the incident waves of both polarizations are considered in the angular range of 130°–180°.

3.3.2. Lossy Spheres

Subsequently, a two-layered dielectric lossy sphere is considered. The results of the values of $\tau_C^{(+)}$ and $\tau_L^{(l)}$ are also shown, as in Fig. 8 and Fig. 9. The figures show that when the size of the outer layer increases, a number of oscillations of the value for $\tau_C^{(+)}$ are observed. Considering the linearly polarized incident wave, if the size of the out layer is fixed, when the radius of the inner sphere decreases, the minimum value of $\tau_L^{(l)}$ at about 127° become smaller. While the radius of the outer layer increases and the size of inner layer is set to be constant, the

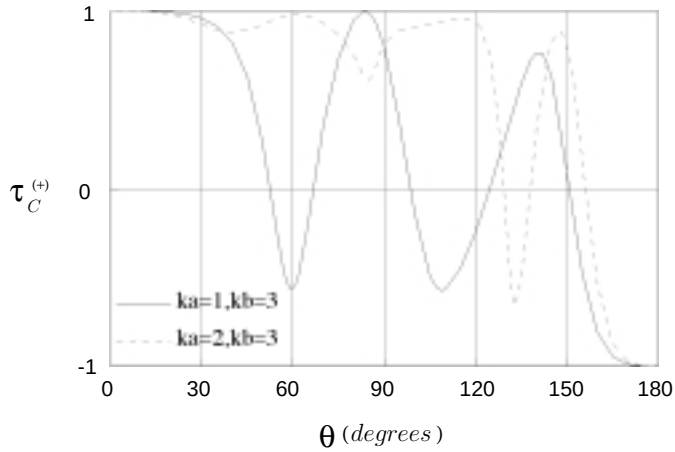

(a) $ka = (1, 2);\ kb = (3, 3)$

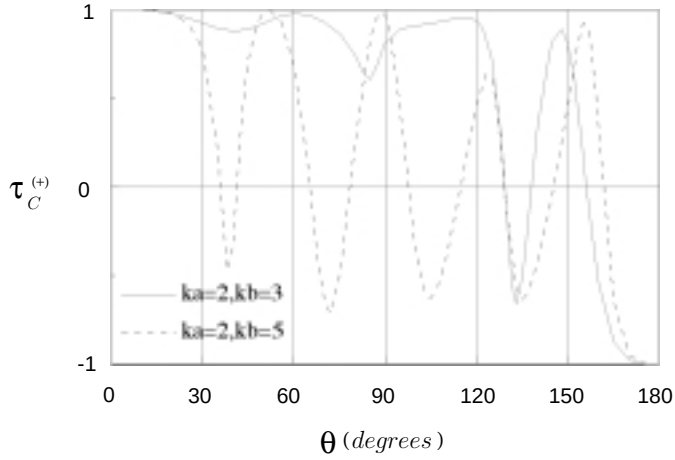

(b) $ka = (2, 2);\ kb = (3, 5)$

Figure 5. The value of $\tau_C^{(+)}$ for a sphere of different sizes. The parameters used here are $\epsilon_{s2} = 3.0$, $\epsilon_{s3} = 5.0$ μ_{s2}=1.5, μ_{s3}=2.0, and $k_r = 0.1$. (a) Comparison between the results for a two-layered dielectric sphere with $ka = 1$ and $kb = 3$ and that with $ka = 2$ and $kb = 3$. (b) Comparison between the results for a two layered dielectric sphere with $ka = 2$ and $kb = 3$ and that with $ka = 2$ and $kb = 5$.

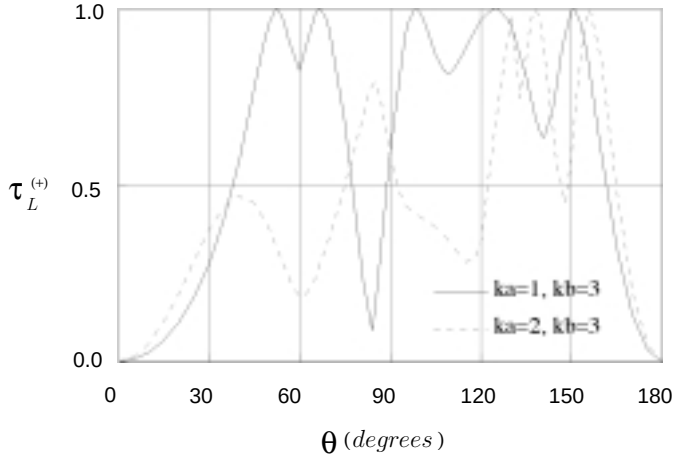

(a) $ka = (1, 2);\ kb = (3, 3)$

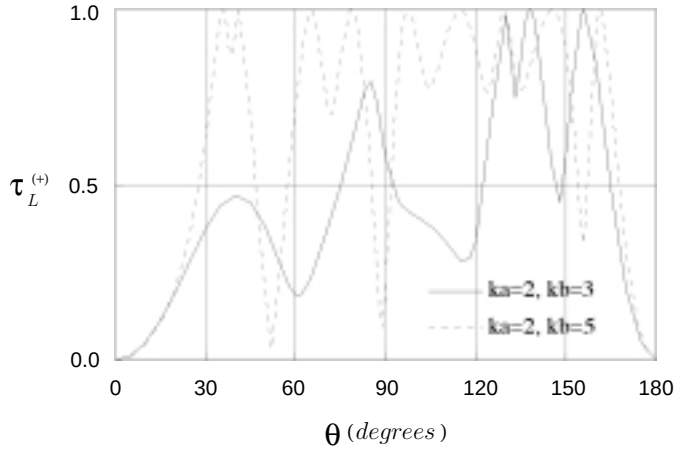

(b) $ka = (2, 2);\ kb = (3, 5)$

Figure 6. The value of $\tau_L^{(+)}$ for a sphere of different sizes. The parameters used are $\epsilon_{s2} = 3.0$, $\epsilon_{s3} = 5.0$ $\mu_{s2} = 1.5$, $\mu_{s3} = 2.0$ and $k_r = 0.1$. (a) Comparison between the results for a two layered dielectric sphere with $ka = 1$ and $kb = 3$ and that of $ka = 2$ and $kb = 3$. (b) Comparison between the results for a two layered dielectric sphere with $ka = 2$ and $kb = 3$ and that with $ka = 2$ and $kb = 5$.

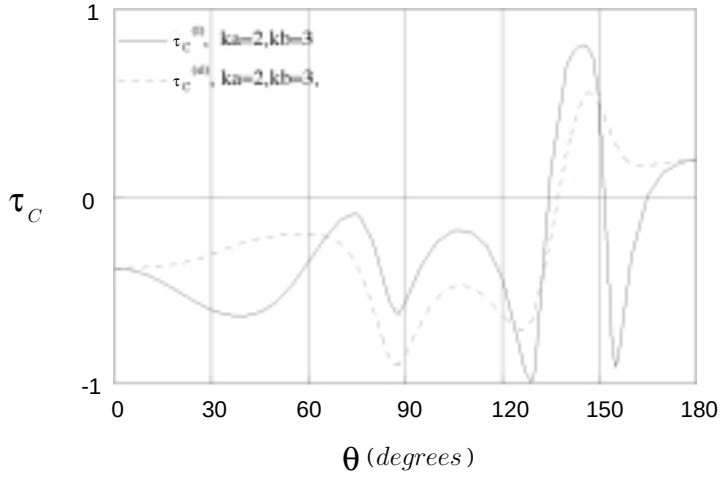

(a) The value of τ_C

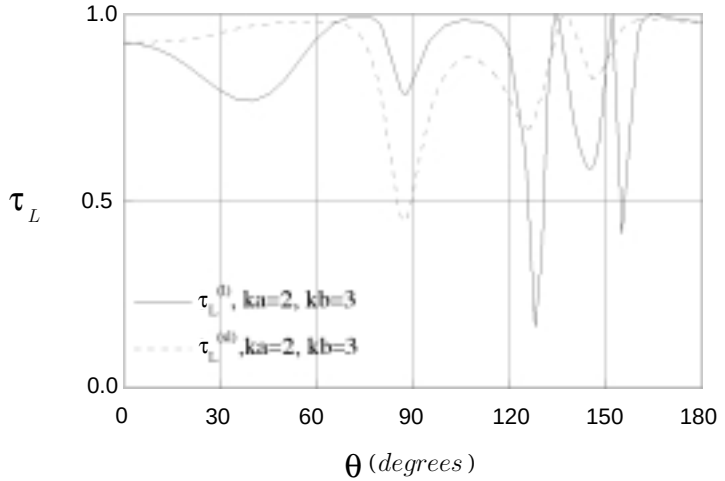

(b) The value of τ_L

Figure 7. The values of $\tau_C^{(l)}$, $\tau_C^{(sl)}$, $\tau_L^{(l)}$ and $\tau_L^{(sl)}$ in the $\phi = 0$ plane for a two-layered dielectric sphere. The parameters used are $\epsilon_{s2} = 3.0$, $\epsilon_{s3} = 5.0$ μ_{s2}=1.5, $\mu_{s3} = 2.0$ and $k_r = 0.1$. (a) τ_C for the two-layered sphere with $ka = 2$ and $kb = 3$. (b) τ_L for the two-layered sphere with $ka = 2$ and $kb = 3$.

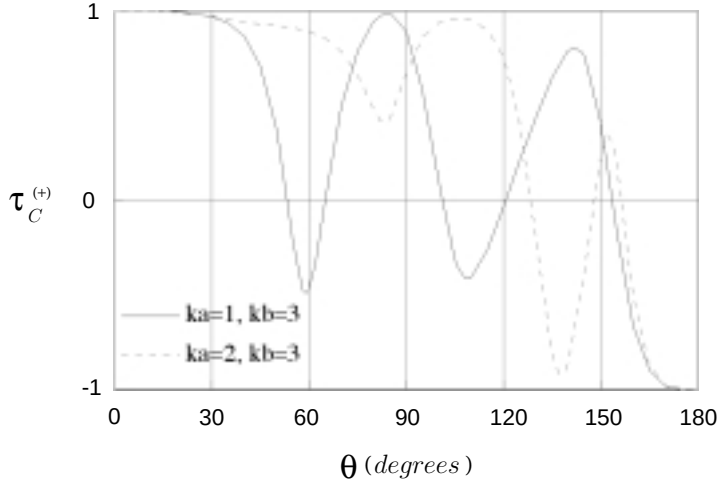

(a) $ka = (1, 2)$ and $kb = (3, 3)$

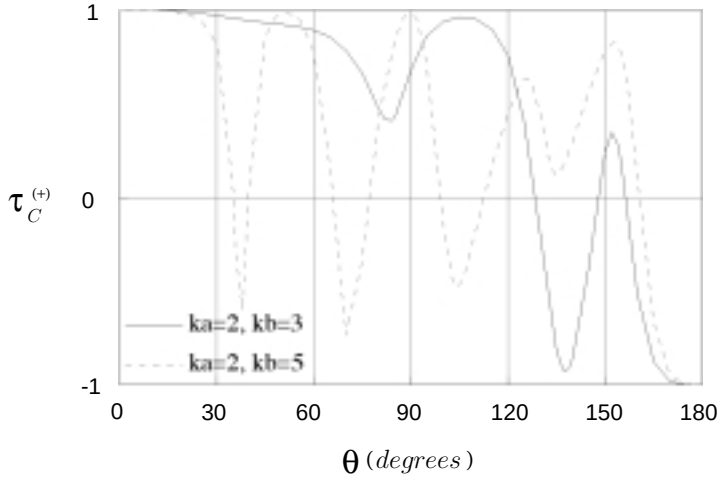

(b) $ka = (2, 2)$ and $kb = (3, 5)$

Figure 8. The value of $\tau_C^{(+)}$ for a sphere of different sizes. The parameters used are $\epsilon_{s2} = 3.0{+}0.15i$, $\epsilon_{s3} = 5.0{+}0.1i$, μ_{s2}=1.5, μ_{s3}=2.0 and $k_r = 0.1$. (a) Comparison between the results for a two layered dielectric sphere with $ka = 1$ and $kb = 3$ and that with $ka = 2$ and $kb = 3$. (b) Comparison between the results for a two layered dielectric sphere with $ka = 2$ and $kb = 3$ and that with $ka = 2$ and $kb = 5$.

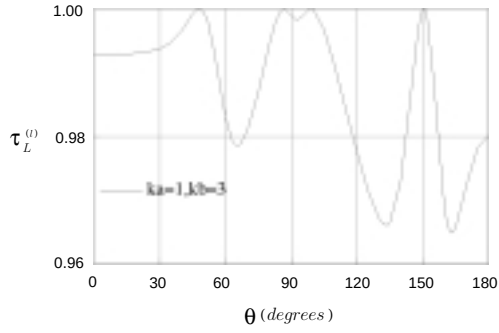

(a) $ka = 1$ and $kb = 3$

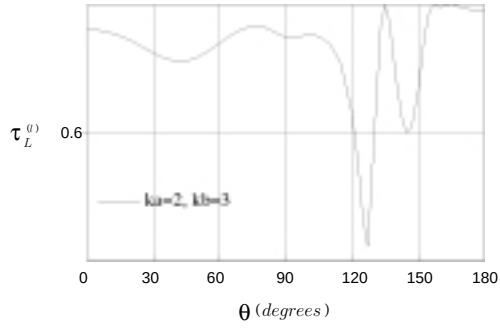

(b) $ka = 2$ and $kb = 3$

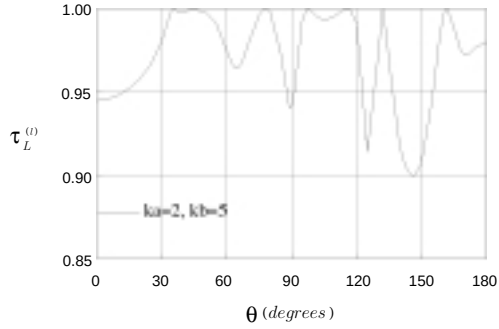

(c) $ka = 2$ and $kb = 5$

Figure 9. The value of $\tau_L^{(l)}$ in $\phi = 0$-plane for a sphere of different sizes. The parameters used are $\epsilon_{s2} = 3.0 + 0.1i$, $\epsilon_{s3} = 5.0 + 0.15i$, μ_{s2}=1.5, μ_{s3}=2.0 and $k_r = 0.1$. (a) Comparison between the results for a two layered dielectric sphere with $ka = 1$ and $kb = 3$ and that with $ka = 2$ and $kb = 3$. (b) Comparison between the results for a two layered dielectric sphere with $ka = 2$ and $kb = 3$ and that with $ka = 2$ and $kb = 5$.

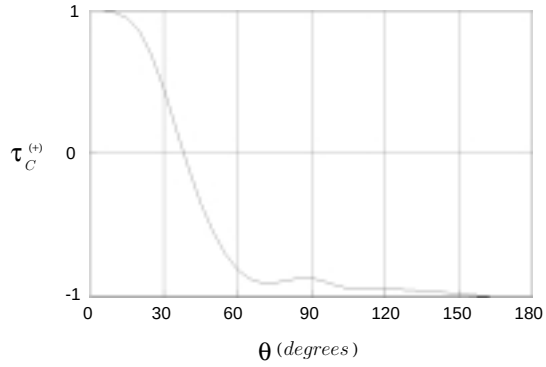

(a) The value of $\tau_C^{(+)}$

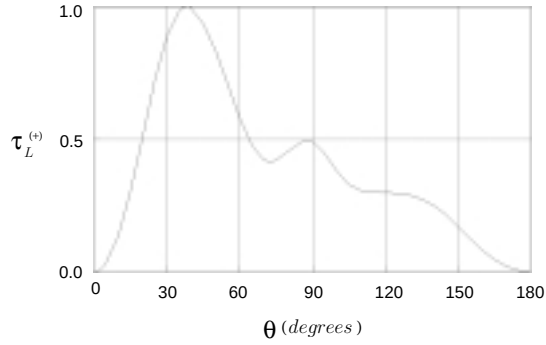

(b) The value of $\tau_L^{(+)}$

Figure 10. The values of $\tau_C^{(+)}$ and $\tau_L^{(+)}$ versus θ in degrees for a conducting sphere coated with a dielectric out layer. $ka = 1$ and $kb = 3$, where a is the radius of the conducting sphere and $b - a$ is the thickness of the dielectric coated layer. The material parameters of the coated layer are $3.0\epsilon_0$, $2.0\mu_0$, and $k_r = 0.1$.

minimum values of $\tau_L^{(l)}$ at 127° and 145° are decreased. Physically, these phenomena are expected. By changing the observation direction for the bi-static radar system, one may actually control the polarization of the scattered waves.

3.4. Scattering by a Conducting Sphere Coated with a Dielectric Layer

The last case is the scattering by the conducting sphere with a dielectric coated layer, where $\tau_C^{(+)}$,$\tau_L^{(+)}$, $\tau_C^{(l)}$, $\tau_C^{(sl)}$,$\tau_L^{(l)}$and $\tau_L^{(sl)}$ are calculated.

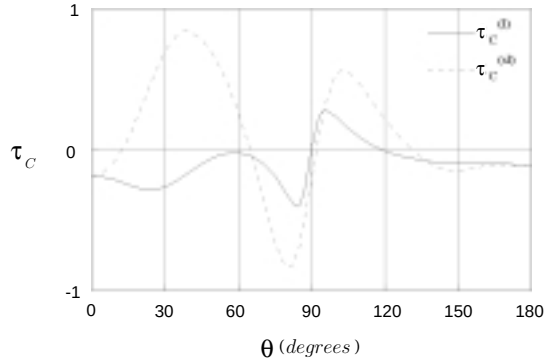

(a) The value of τ_C

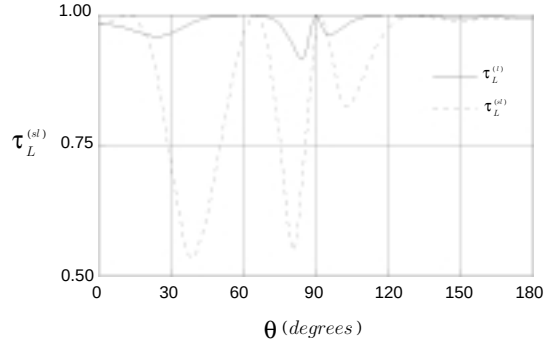

(b) The value of τ_L

Figure 11. Comparison between the results of $\tau_{C,L}^{(l)}$ and $\tau_{C,L}^{(sl)}$ for the conducting sphere with a dielectric coated layer in the $\phi = 0$ plane.

The results are shown from Fig. 10 to Fig. 11. When both of the first and second polarization incident waves are considered, the value of $\tau_C^{(sl)}$ is greater than $\tau_C^{(l)}$ in the ranges of 0°–65° and 95°–135° but less than from 65° to 95°. $\tau_L^{(sl)}$ has larger variation against θ in degrees than $\tau_L^{(l)}$ and the values of $\tau_L(sl)$ are less than $\tau_L^{(l)}$ in nearly the whole angular range.

To gain an insight into the effects of increasing chiral parameter, we calculated τ_C and τ_L for different cases. It is shown in Fig. 12 that when chiral parameter increases, the difference between our results and those in [21] is significant. In the second case, as the chiral parameter increases, the oscillation of both $\tau_C^{(l)}$ and $\tau_L^{(sl)}$ is strengthened as

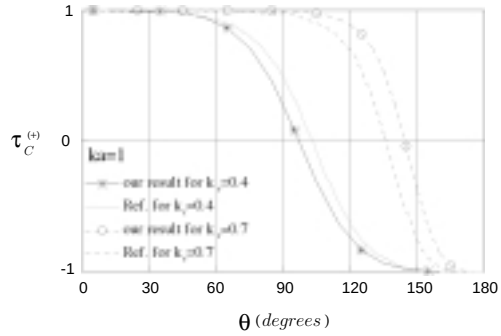

(a) The value of $\tau_C^{(+)}$ for $k_r = 0.4$ and 0.7

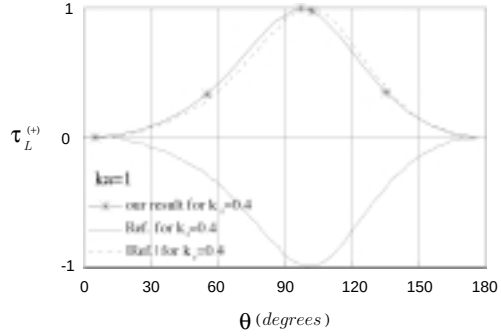

(b) The value of $\tau_L^{(+)}$ for $k_r = 0.4$

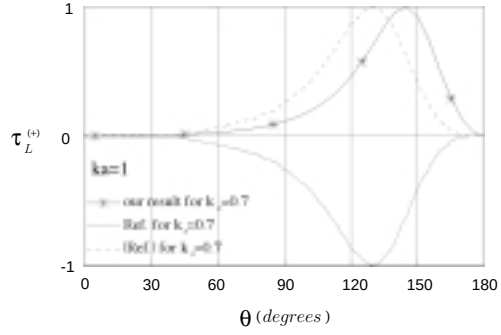

(c) The value of $\tau_L^{(+)}$ for $k_r = 0.7$

Figure 12. (a) Comparison between the results of $\tau_C^{(+)}$ of a single layered achiral sphere for different chiral parameters of $k_r = 0.4$ and $k_r = 0.7$. (b) Comparison between the results of $\tau_L^{(+)}$ for a chiral parameter of $k_r = 0.4$. (c) Comparison between the results of $\tau_L^{(+)}$ for a chiral parameter of $k_r = 0.7$.

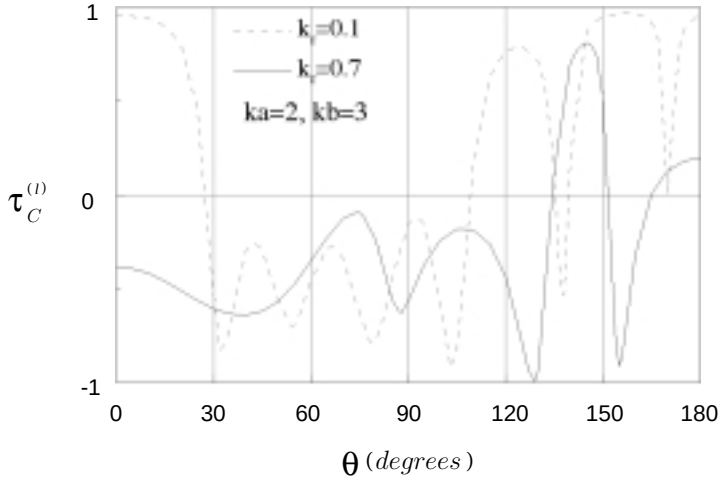

(a) The value of $\tau_C^{(l)}$

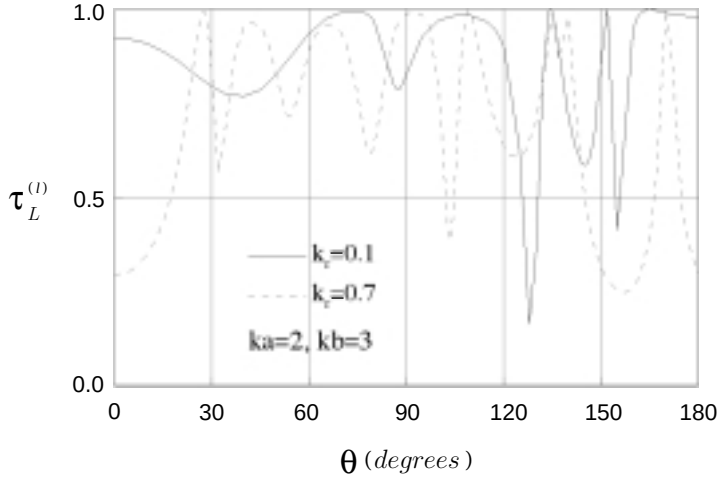

(b) The value of $\tau_L^{(l)}$

Figure 13. (a) Comparison between the results of $\tau_C^{(l)}$ for the two-layered dielectric sphere for different chiral parameters of $k_r = 0.1$ and $k_r = 0.7$. (b) Comparison between the results of $\tau_L^{(l)}$ for different chiral parameters of $k_r = 0.1$ and $k_r = 0.7$. All in the $\phi = 0$ plane.

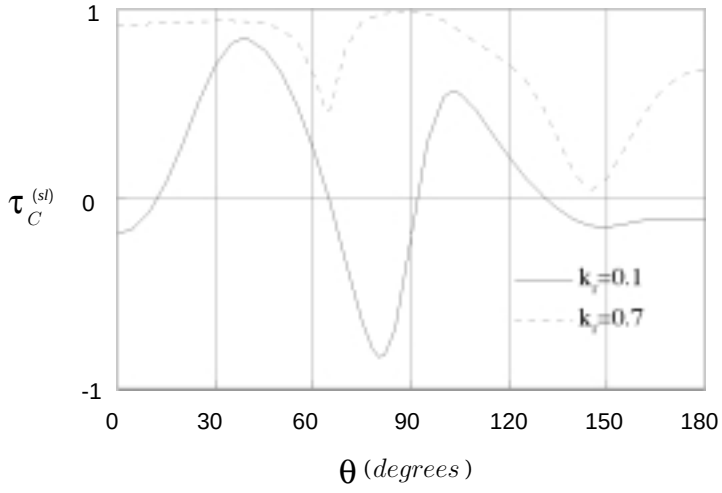

(a) $\tau_C^{(sl)}$ for $k_r = 0.1$ and 0.7

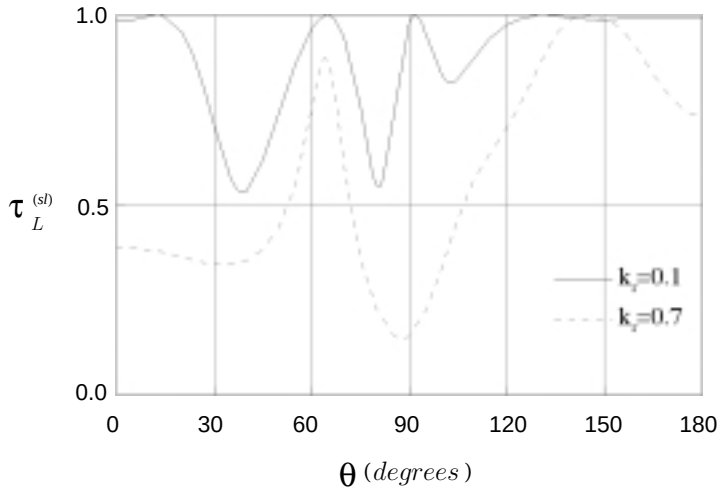

(b) $\tau_L^{(sl)}$ for $k_r = 0.1$ and 0.7

Figure 14. (a) Comparison between the results of $\tau_C^{(sl)}$ in the $\phi = 0$ plane for the conducting sphere with a dielectric coated layer for chiral parameters $k_r = 0.1$ and $k_r = 0.7$. (b) Comparison between the results of $\tau_L^{(sl)}$ for different chiral parameters of $k_r = 0.1$ and $k_r = 0.7$ in the $\phi = 0$ plane.

shown in Fig. 13. For the last case in Fig. 14, the values of $\tau_C^{(sl)}$ increase while the values of $\tau_L^{(sl)}$ decrease when the chiral parameter increases. It has shown that the chirality plays an important role in the characteristics of the scattered fields. Physically, it is seen that there exists sometimes a window within which the radio wave has only the circular or linear polarization. This means that we can vary the chiral medium parameters and tune the physical dimensions of a practical optical or electromagnetic system so as to achieve the desired polarization that the system requires.

4. CONCLUSION

This paper has presented an efficient technique (*i.e.*, the radiation-to-scattering transform method) to investigate, and an analytic solution to, the problem of electromagnetic scattering by an achiral sphere immersed in a host chiral medium. The coupled wave equations for chiral media were transformed into a set of decoupled wave equations so that the chiral media can be decomposed into two kinds of isotropic materials which evolve different circular polarizations. Two kinds of sources which are assumed to locate at infinity and to generate the incident waves of different polarizations are found and their distributions at infinity are formulated. Also, the dyadic Green's functions for the two structures considered here are formulated and their scattering coefficients are derived for the first time in the literature. Based on the radiation-to-scattering transform, the scattered fields have been found, and both the circularly polarized and linearly polarized incident waves are considered. The degrees of circular polarization and linear polarization are numerically computed and compared with the existing approximate results. Numerical results illustrate various effects of chirality and dimension of the (layered) sphere. This method *newly developed in this paper* is quite straightforward, rigorous and easy-to-use for a multilayered sphere of an arbitrary numbers of layers. From the full-wave results, some new physical phenomena of the electromagnetic scattering are revealed through numerical discussions.

APPENDIX A. SCATTERING COEFFICIENTS IN EQ. (12)

The scattering coefficients in Eq. (12) have been found in [10] but are provided here as self-contained information for readers' convenience

and ease of reading and re-derivations:

$$\mathcal{C}_{12}^{11} = -\left(k_1^{(R)}\right)^2 \frac{\mathcal{T}_{13}^{(1)}\mathcal{T}_{22}^{(1)} - \mathcal{T}_{23}^{(1)}\mathcal{T}_{12}^{(1)}}{\mathcal{T}_{11}^{(1)}\mathcal{T}_{22}^{(1)} - \mathcal{T}_{12}^{(1)}\mathcal{T}_{21}^{(1)}}, \tag{A1}$$

$$\mathcal{C}_{14}^{11} = -\left(k_1^{(l)}\right)^2 \frac{\mathcal{T}_{14}^{(1)}\mathcal{T}_{22}^{(1)} - \mathcal{T}_{24}^{(1)}\mathcal{T}_{12}^{(1)}}{\mathcal{T}_{11}^{(1)}\mathcal{T}_{22}^{(1)} - \mathcal{T}_{12}^{(1)}\mathcal{T}_{21}^{(1)}}, \tag{A2}$$

$$\mathcal{C}_{22}^{11} = -\left(k_1^{(R)}\right)^2 \frac{\mathcal{T}_{23}^{(1)}\mathcal{T}_{11}^{(1)} - \mathcal{T}_{13}^{(1)}\mathcal{T}_{21}^{(1)}}{\mathcal{T}_{11}^{(1)}\mathcal{T}_{22}^{(1)} - \mathcal{T}_{12}^{(1)}\mathcal{T}_{21}^{(1)}}, \tag{A3}$$

$$\mathcal{C}_{24}^{11} = -\left(k_1^{(l)}\right)^2 \frac{\mathcal{T}_{24}^{(1)}\mathcal{T}_{11}^{(1)} - \mathcal{T}_{14}^{(2)}\mathcal{T}_{21}^{(1)}}{\mathcal{T}_{11}^{(1)}\mathcal{T}_{22}^{(1)} - \mathcal{T}_{12}^{(1)}\mathcal{T}_{21}^{(1)}}, \tag{A4}$$

where The intermediates, $\mathcal{T}_{ij}^{(1)}$ (where $i = 1$ or 2 while $j = 1, 2, 3$, or 4), are obtained from

$$\mathbf{T}^{(1)} = \left[\mathcal{T}_{j\ell}^{(1)}\right]_{4\times 4} = [\mathbf{T}_{N-1}][\mathbf{T}_{N-2}]\cdots[\mathbf{T}_2][\mathbf{T}_1]. \tag{A5}$$

The matrix $\mathbf{T_f}$ is defined as:

$$\mathbf{T}_f = \mathbf{F}_{f+1}^{-1}\mathbf{F}_f = \left[T_{j\ell}^{(f)}\right]_{4\times 4}, \tag{A6}$$

where

$$\mathbf{F}_f = \begin{bmatrix} \partial\hbar_{ff}^{(r)} & -\partial\hbar_{ff}^{(l)} & \partial\Im_{ff}^{(r)} & -\partial\Im_{ff}^{(l)} \\ \hbar_{ff}^{(r)} & \hbar_{ff}^{(l)} & \Im_{ff}^{(r)} & \Im_{ff}^{(l)} \\ \eta_f^{-1}\partial\hbar_{ff}^{(r)} & \eta_f^{-1}\partial\hbar_{ff}^{(l)} & \eta_f^{-1}\partial\Im_{ff}^{(r)} & \eta_f^{-1}\partial\Im_{ff}^{(l)} \\ \eta_f^{-1}\hbar_{ff}^{(r)} & -\eta_f^{-1}\hbar_{ff}^{(l)} & \eta_{fc}^{-1}\Im_{ff}^{(r)} & -\eta_f^{-1}\Im_{ff}^{(l)} \end{bmatrix}; \tag{A7}$$

and the notations in the above matrix are defined as follows:

$$\Im_{im}^{(r,l)} = j_n(k_i^{(r,l)}a_m), \tag{A8}$$

$$\hbar_{im}^{(r,1)} = h_n^{(2)}(k_i^{(r,l)}a_m), \tag{A9}$$

$$\partial\Im_{im}^{(r,l)} = \frac{1}{\rho}\frac{d[\rho j_n(\rho)]}{d\rho}\bigg|_{\rho=k_i^{(r,l)}a_m}, \tag{A10}$$

$$\partial\hbar_{im}^{(r,1)} = \frac{1}{\rho}\frac{d[\rho h_n^{(2)}(\rho)]}{d\rho}\bigg|_{\rho=k_i^{(r,l)}a_m}; \tag{A11}$$

$$i = 1, 2, \cdots, N,$$

$$m = 1, 2, \cdots, N-1;$$

with the reciprocal of the wave impedance given by:

$$\eta_f^{-1} = \sqrt{\frac{\varepsilon_f}{\mu_f}}. \tag{A12}$$

REFERENCES

1. Jaggard, D. L., A. R. Mickelson, and C. H. Papas, "On electromagnetic waves in chiral media," *Appl. Phys.,* Vol. 18, 211–216, 1978.
2. Silverman, M. P., "Reflection and refraction at the surface of a chiral medium," *J. Opt. Soc. Am. A,* Vol. 3, 830–837, 1986.
3. Vegni, L., R. Cicchetti, and P. Capece, "Spectral dyadic Green's function formulation for planar integrated structures," *IEEE Trans. Antennas Propagat.,* Vol. AP-36, No. 8, 1057–1065, 1988.
4. Engheta, N. and P. Pelet, "Modes in chirowaveguides," *Opt. Lett.,* Vol. 14, 593–595, 1990.
5. Engheta N. and M. W. Kowarz, "Antenna radiation in the presence of a chiral sphere," *J. Appl. Phys.,* Vol. 67, No. 2, 639–647, 1990.
6. Wei, R., "Dyadic Green's functions and dipole radiations in layered chiral media," *J. Appl. Phys.,* Vol. 75, No. 1, 30–35, Jan. 1994.
7. Ali, S. M., T. M. Habashy, and J. A. Kong, "Spectral-domain dyadic Green's function in layered chiral media," *J. Opt. Soc. Am. A,* Vol. 9, No. 3, 413–423, March 1992.
8. Bassiri, S., C. H. Papas, and N. Engheta, "Electromagnetic wave propagation through a dielectric-chiral interface and through a chiral slab," *J. Opt. Soc. Am. A,* Vol. 5, 1450–1459, 1988.
9. Lakhtakia, A., V. V. Varadan, and V. K. Varadan, "Field equations, Huygens's principle, integral equations, and theorems for radiation and scattering of electromagnetic waves in isotropic chiral media," *J. Opt. Soc. Am. A,* Vol. 5, 175–184, 1988.
10. Li, L.-W., P. S. Kooi, M.-S. Leong, and T.-S. Yeo, "A general expression of dyadic Green's function in radially multilayered chiral media," *IEEE Trans. Antennas Propagat.,* Vol. 43, No. 3, 232–238, March 1995.
11. Li, L.-W., D. You, M.-S. Leong, and J. A. Kong, "Electromagnetic scattering by an inhomogeneous chiral sphere of nonlinear varying permittivity: A discrete analysis using multilayered model," *Progress In Electromagnetics Research,* Vol. 23, EMW Publishing, Cambridge, Boston, 1999.

12. Bohren, C. F., "Light scattering by an optically active sphere," *Chem. Phys. Lett.,* Vol. 29, 458–462, 1974.
13. Lakhtakia, A., V. K. Varadan, and V. V. Varadan, "Scattering and absorption characteristics of lossy dielectric, chiral, nonspherical objects," *Appl. Opt.,* Vol. 24, 4146–4154, 1985.
14. Rojas, R. G., "Integral equations for the scattering by a three dimensional inhomogeneous chiral body," *J. Electromagn. Waves Applic.,* Vol. 6, No. 5/6, 733–750, 1992.
15. Bohren, C. F., "Scattering of electromagnetic waves by an optically active cylinder," *J. Colloid Interface Sci.,* Vol. 66, 101–109, 1974.
16. Kluskens, M. S. and E. H. Newman, "Scattering by a multilayer chiral cylinder," *IEEE Trans. Antennas Propagat.,* Vol. AP-39, 91–96, 1991.
17. Graglia, R. D., P. L. E. Uslenghi, and C. L. Yu, "Electromagnetic oblique scattering by a cylinder coated with chiral layers and anisotropic jump-immittance sheets," *J. Electromagn. Waves Applic.,* Vol. 6, No. 5/6, 695–719, 1992.
18. Chen, Z., W. Hong, and W. Zhang, "Electromagnetic scattering from a chiral cylinder-general case," *IEEE Trans. Antrnnas Propag.,* Vol. 44, No. 7, 912–917, 1996.
19. Bohren, C. F., "Scattering of electromagnetic waves by an optically active spherical shell," *J. Chem. Phys.,* Vol. 62, 1566–1571, 1975.
20. Cooray, M. F. and I. R. Ciric, "Wave scattering by a chiral spheroid," *J. Opt. Soc. Am. A,* Vol. 10, No. 6, 1197–1203, June 1993.
21. Lindell, I. V. and M. P. Silverman, "Plane-wave scattering from a nonchiral object in a chiral environment," *J. Opt. Soc. Am. A,* Vol. 14, No. 1, 79–90, Jan., 1997.
22. Godlevskaya, A. N. and V. N. Kapshai, "Scattering of electromagnetic waves on spherically symmetrical particles in a naturally gyrotropic medium," *Optics and Spectroscopy,* Vol. 68, No. 1, 69–72, Jan. 1990.
23. Afonin, A. A., A. N. Godlevskaya, V. N. Kapshai, S. P. Kurlovich, and A. N. Serdyokov, "Scattering of electromagnetic waves by a two-layer spherical particle in a naturally gyrotropic medium," *Optics and Spectroscopy,* Vol. 69, No. 2, 242–245, Feb. 1990.
24. Lakhtakia, A., *Beltrami Fields in Chiral Media,* World Scientific, Singapore, 1994.
25. Li, L.-W., D. You, M.-S. Leong, T.-S. Yeo, and J. A. Kong, "Elec-

tromagnetic scattering by multilayered chiral-media structures: A scattering-to-radiation transform," *Progress In Electromagnetics Research,* Vol. 26, EMW Publishing, Cambridge, Boston, 2000.

26. Lindell, I. V., A. H. Sihvola, S. A. Tretyakov, and A. J. Viitanen, *Electromagnetic Waves in Chiral and Bi-Isotropic Media,* Artech House, Boston, 1994.
27. Bassiri, S., N. Engheta, and C. H. Papas, "Dyadic Green's function and dipole radiation in chiral media," *Alta Freq.,* Vol. 55, 83–88, 1986.
28. Wolfram, S., *Mathematica,* the 4th edition, Cambridge University Press, New York, 1999.
29. Li, L.-W., T.-S. Yeo, P. S. Kooi, and M.-S. Leong, "An efficient calculational approach to evaluation of microwave specific attenuation," *Accepted by IEEE Trans. Antennas Propagat.,* December 1999.
30. Ishimaru, A., *Wave Propagation and Scattering in Random Media,* Vols. 1 & 2, Academic Press, New York, 1978.